Global Change Biology **WILEY**

RESEARCH ARTICLE

Soil carbon and nitrogen cycling at the atmosphere–soil interface: Quantifying the responses of biocrust–soil interactions to global change

K. Witzgall[1] | B. D. Hesse[2,3] | N. L. Pacay-Barrientos[1] | J. Jansa[4] |
O. Seguel[5] | R. Oses[6] | F. Buegger[7] | J. Guigue[1] | C. Rojas[8,9] | K. Rousk[10] |
T. E. E. Grams[2] | N. Pietrasiak[11] | C. W. Mueller[1,12,13]

[1]Soil Science, TUM School of Life Sciences, Technical University of Munich, Freising-Weihenstephan, Germany

[2]Land Surface Atmosphere Interactions – AG Ecophysiology of Plants, TUM School of Life Sciences, Technical University of Munich, Freising-Weihenstephan, Germany

[3]Institute of Botany (BOT), University of Natural Resources and Life Sciences, Vienna, Austria

[4]Institute of Microbiology, Czech Academy of Sciences, Prague, Czech Republic

[5]Facultad de Ciencias Agronómicas, Universidad de Chile, Santiago, Chile

[6]Centro Regional de Investigación y Desarrollo Sustentable de Atacama (CRIDESAT), Universidad de Atacama, Copiapó, Chile

[7]Research Unit Environmental Simulation, Helmholtz Zentrum München (GmbH), German Research Center for Environmental Health, Neuherberg, Germany

[8]Laboratory of Soil Microbial Ecology and Biogeochemistry (LEMiBiS), Universidad de O'Higgins, San Fernando, Chile

[9]Center of Applied Ecology and Sustainability (CAPES), Santiago, Chile

[10]Department of Biology, Terrestrial Ecology Section, University of Copenhagen, Copenhagen, Denmark

[11]Department of Plant and Environmental Sciences, New Mexico State University, Las Cruces, New Mexico, USA

[12]Institute for Ecology, Chair of Soil Science, Technical University Berlin, Berlin, Germany

Abstract

In drylands, where water scarcity limits vascular plant growth, much of the primary production occurs at the soil surface. This is where complex macro- and microbial communities, in an intricate bond with soil particles, form biological soil crusts (biocrusts). Despite their critical role in regulating C and N cycling in dryland ecosystems, there is limited understanding of the fate of biologically fixed C and N from biocrusts into the mineral soil, or how climate change will affect C and N fluxes between the atmosphere, biocrusts, and subsurface soils. To address these gaps, we subjected biocrust–soil systems to experimental warming and drought under controlled laboratory conditions, monitored CO_2 fluxes, and applied dual isotopic labeling pulses ($^{13}CO_2$ and $^{15}N_2$). This allowed detailed quantification of elemental pathways into specific organic matter (OM) pools and microbial biomass via density fractionation and phospholipid fatty acid analyses. While biocrusts modulated CO_2 fluxes regardless of the temperature regime, drought severely limited their photosynthetic C uptake to the extent that the systems no longer sustained net C uptake. Furthermore, the effect of biocrusts extended into the underlying 1 cm of mineral soil, where C and N accumulated as mineral-associated OM ($MAOM_{<63\mu m}$). This was strongly associated with increased relative dominance of fungi, suggesting that fungal hyphae facilitate the downward C and N translocation and subsequent MAOM formation. Most strikingly, however, these pathways were disrupted in systems exposed to warming, where no effects of biocrusts on the elemental composition of the underlying soil nor on MAOM were determined. This was further associated with reduced net biological N fixation under combined warming and drought, highlighting how changing climatic conditions diminish some of the most fundamental ecosystem functions of biocrusts, with detrimental repercussions for C and N cycling and the persistence of soil organic matter pools in dryland ecosystems.

[13]Department of Geosciences and Natural Resource Management, University of Copenhagen, Copenhagen, Denmark

Correspondence
Kristina Witzgall, Soil Science, TUM School of Life Sciences, Technical University of Munich, Freising-Weihenstephan, Germany.
Email: kristina.witzgall@tum.de

1 | INTRODUCTION

In drylands, which constitute almost half of the Earth's terrestrial surface, water scarcity constrains the growth of vascular plants. Instead, primary production occurs directly at the soil surface by biological soil crusts (biocrusts) which establish at the top few millimeters of soil. These thin and well-aggregated surface layers are formed by communities, composed of non-vascular photoautotrophs (e.g., bryophytes, lichens, and cyanobacteria) and microbial heterotrophs (e.g., fungi and bacteria) living in intricate association with soil mineral particles (Weber et al., 2022). They can comprise over 70% of the living cover in drylands and are critical contributors to ecosystem functionality at multiple scales (Belnap & Lange, 2001; Maestre et al., 2013; Weber et al., 2016). At local scales, biocrusts regulate nutrient cycling (Belnap et al., 2016), soil food web structures (Mager & Thomas, 2011), subsurface soil microbial communities (Bates et al., 2010; Xiao & Veste, 2017), water infiltration (Barger et al., 2006; Chamizo et al., 2012; Kidron et al., 2022), and soil surface stabilization (Felde et al., 2018; Pietrasiak et al., 2013; Pointing & Belnap, 2014). At broader scales, the fixation of atmospheric CO_2 and N_2 represents a major component of biogeochemical fluxes with implications for global C and N cycles (Belnap, 2001; Finger-Higgens et al., 2022; Weber et al., 2022), estimated to account for 7% of total net C uptake and 50% of terrestrial N_2 fixation (Elbert et al., 2012). At the same time, biocrusts can also contribute significantly to C losses via stimulated soil respiration, thereby driving both C gains and losses in dryland ecosystems (Castillo-Monroy et al., 2011).

Biocrusts are characterized by an intricate association between biotic components and the soil matrix. This can be attributed to two central mechanisms: (i) the direct structural enmeshment of soil particles by filamentous strands of cyanobacteria, moss rhizoids, and fungal hyphae (Barger et al., 2006; Weber et al., 2022) and (ii) the release of extracellular polymeric substances (EPS) contributing to the formation of aggregated structures at the soil surface (Mager & Thomas, 2011; Chenu & Consentino, 2011; Costa et al., 2018). Given the otherwise low organic C and N contents in dryland soils, these compounds further represent a major source of easily available energy and nutrients to microbial surface communities and can constitute up to 75% of the total soil organic C (SOC) stocks (Mager, 2010;

Mager & Thomas, 2011; Rossi & De Philippis, 2015). This build-up of C can also impact the subcrust soil, for example, via leaching of dissolved nutrients (Young et al., 2022), litter inputs of decomposing biocrust biomass (Hagemann & Moroni, 2015), or via the production and release of microbial exometabolites (Swenson et al., 2018). However, there are still major uncertainties around the elemental pathways from, and overall contribution of, biocrust to different soil organic matter (SOM) pools and SOC storage.

Along with the recognition of biocrusts as critical components in dryland ecosystem functionality across various scales, there is growing concern for their susceptibility to climate change (e.g., Darrouzet-Nardi et al., 2015; Elbert et al., 2012; Finger-Higgens et al., 2022; Maestre, Cristina, et al., 2015; Maphangwa et al., 2012; Permin et al., 2022; Rodríguez-Caballero et al., 2018; Tucker et al., 2020; Xu et al., 2022). Similar to the effects of anthropogenic disturbances, climate change can cause well-developed biocrusts to regress to early-successional and species-poor communities, significantly compromising their capacity to fix C and N (Ferrenberg et al., 2015; Housman et al., 2006; Lange, 2001; Tucker et al., 2019). Evaporative stress and increasing aridity associated with warming temperatures have also been shown to increase moss mortality (Ladrón de Guevara et al., 2018; Maestre et al., 2013), decline the abundance and diversity of fungi and bacteria (Maestre, Delgado-Baquerizo, et al., 2015; Rodríguez et al., 2024), and reduce the cover of N-fixing lichens (Finger-Higgens et al., 2022). Moreover, a growing body of evidence shows how warming coupled with infrequent precipitation diminishes the photosynthetic capacity of biocrusts, compromising their ability to maintain net C uptake (Maestre et al., 2013; Reed et al., 2012; Tucker et al., 2020). This means that biocrust–soil systems may no longer function as net C sinks (Darrouzet-Nardi et al., 2015) which has fundamental consequences for several ecosystem services, redefining the future role and functionality of biocrusts in drylands (Garcia-Pichel et al., 2013; Reed et al., 2012). Yet, despite increased research attention, our understanding of the repercussions of global change on biocrusts is still in its infancy, particularly beyond the effects within the borders of the biocrust layer. Only recently has more attention been directed to implications on biocrust–soil interactions, such as the pathways and mechanisms of biocrust-derived C and N into the subsurface soil beneath the biocrust (e.g., Beraldi-Campesi

et al., 2009; Ferrenberg et al., 2018; Maestre et al., 2013; Tucker et al., 2020). In Díaz-Martínez et al., 2023, pioneered the study of particulate (POM) and mineral-associated organic matter (MAOM) formation within the biocrust layer, marking an important contribution for our understanding of OM dynamics in biocrust systems. Yet, how their findings compare to SOM dynamics in the underlying mineral soil is unknown.

In this study, we aim to extend the understanding of how changing climatic conditions impact fundamental biogeochemical cycles in dryland biocrust–subsurface soil systems (biocrust–soil systems hereafter) at the process level by tracing C and N from biocrusts into the underlying mineral soil. This was realized in a phytotron climate simulation experiment, where biocrust–soil systems were exposed to warming (+5°C) and/or drought (−50% water addition) under controlled laboratory conditions. In addition to monitoring CO_2 fluxes, repeated $^{13}CO_2$ and $^{15}N_2$ labeling pulses were applied to directly disentangle interactions between biocrusts, microorganisms, and soil. The allocation of biocrust-derived C and N into POM and MAOM (density fractionation) and C into microbial biomass (phospholipid fatty acid [PLFA] analysis) was determined both within the biocrust layer and in the underlying 1 cm thick subsurface soil, allowing us to distinguish biocrust effects that extend into the mineral soil. We hypothesize that (i) biocrusts contribute to the build-up of soil C and N in the underlying 1 cm soil, (ii) these elemental pathways are impaired in systems exposed to drought and warming and that (iii) the overall biological fixation of C and N is reduced by the applied climate change factors. This systemic approach of the present study, tracing biocrust-derived C and N into specific SOM pools via microbial transformation, provides novel insights into biocrusts as regulators of soil C and N cycles and how changing climatic conditions alter—or even disrupt—fundamental biogeochemical pathways between biocrusts and soils.

2 | MATERIALS AND METHODS

2.1 | Field sampling and soil preparation

Soil was sampled from semiarid Santa Gracia located in the Coastal Cordillera of Chile (−71.166, −29.757; MAT: 13.7°C, MAP: 66 mm; Bernhard et al., 2018; Table S1) from five subplots (10×10 cm), all within 500 m of each other. The subplots were situated on a top slope surrounded by similar vegetation (mainly smaller shrubs, e.g., *Proustia cuneifolia*, *Balbisia peduncularis*, and *Cordia decandra*; Bernhard et al., 2018) classified as "Interior Mediterranean desert scrub" (Luebert & Pliscoff, 2006) and with biocrusts dominated by filamentous cyanobacteria (e.g., *Microcoleus vaginatus* and *Nodosilinea epilithica*; Samolov et al., 2020) but also containing bryophytes, liverworts, and chlorolichens (e.g., *Placidium* sp., *Caloplaca* sp., and *Riccia* spp.; Bernhard et al., 2018). The soil material was collected from two depth layers: 0–1 cm topsoil (A horizon; 77% sand, 13% silt, 10% clay) and 3–5 cm subsoil (B horizon; 77% sand, 12% silt, 11% clay). The biocrust layer was removed prior to sampling, meaning that only the mineral soil substrate was collected in the field. The collected material was sieved (<2 mm) and homogenized into one composite sample for each depth increment (basic soil properties are included in Table S2). The composite samples were then filled into mesocosms (height: 5 cm, Ø: 8 cm, polyvinyl chloride); subsoil material up to 4 cm, and topsoil material in the top 1 cm (1.6 g cm^{-3} bulk density according to field conditions; Riveras-Muñoz et al., 2022; Table S2). The two layers were separated by a strip of Teflon foil to facilitate the separation of the layers after incubation. Each mesocosm was covered from below with mesh (Ø: 30 μm) and placed on elevated metal grids inside incubation vessels (Figure S2).

2.2 | Incubation and experimental setup

The 133-day incubation took place in two phytotron chambers. The control chamber was programmed after climate data collected in the field (10.5–21.5°C; Übernickel et al., 2020) and the warming chamber was continuously set at +5°C (15.5–26.5°C; Figures S1–S3). Photosynthetic photon flux density (PPFD) in both chambers ranged from 65 to 425 μmol m^{-2} s^{-1} during a 14-h photoperiod (Figure S3), set to resemble a cloudy day at the study site (Übernickel et al., 2020). In half of the mesocosms, biocrusts were let to establish spontaneously under water addition (autoclaved deionized H_2O which was gently sprayed across the surface) and light. In the other half, photosynthetic active radiation (PAR) was excluded via shading to prevent biocrust growth, hereafter referred to as bare soil controls (Figure S2). During the first 60 days of incubation, all samples received a total of 6 mL water per day to promote biocrust establishment. During the remaining 73 days, water addition was limited to 1 mL per day (corresponding to the site conditions) in half of the samples, whereas it was reduced by 50% in the other half of the samples (from 1 to 0.5 mL per day), to simulate drought. In summary, this resulted in a total of eight treatments: systems with or without biocrusts (2 levels), ambient and warming temperatures (2 levels), and normal water and reduced water (drought hereafter) conditions (2 levels). A detailed description of the experimental design and incubation can be found in supplements (Figures S1 and S2).

2.3 | Dual isotopic labeling

Both biocrust and bare soil samples underwent repeated $^{13}CO_2$ labeling pulses, achieved by adding an excess of H_2SO_4 to 7.5 mg of 99%$Na_2^{13}CO_3$ (~80 atom% ^{13}C in headspace; Sigma-Aldrich Chemie GmbH, Taufkirchen, Germany) into the sealed incubation vessels for 5-h incubation (Figure S5). Biocrust samples were subjected to one $^{15}N_2$ labeling pulse, by adding 60 mL 99%$^{15}N_2$ (~23 atom% ^{15}N in headspace; Sigma-Aldrich Chemie GmbH, Taufkirchen, Germany) for 8 h to the incubation vessels (further details in supplements; Figure S5). The duration of the $^{15}N_2$ labeling was limited to 8 h to minimize the exposure of the samples to elevated temperature caused by the closed lids (Witzgall et al., 2023). To ensure stable

CO_2 concentrations during labeling, tank CO_2 was added on an hourly basis, adjusted to the individual net CO_2 flux in each sample. Throughout $^{13}CO_2$ and $^{15}N_2$ pulse labeling, PPFD was increased to $600 \, \mu mol \, m^{-2} \, s^{-1}$ to account for the PAR transmittance of the plastic lids ($73.8 \pm 0.3\%$).

2.4 | Respiration and photosynthesis CO_2 flux measurements

In brief, 1 and 0.5 mL of water were added to the respective samples 2.5h before measurement to avoid elevated CO_2 release (Lange, 2001). All samples were flushed with air with a defined CO_2 concentration (>15 min; 405 ppm; −38.3‰ $\delta^{13}C$ V-PDB) and CO_2 samples were collected after 45 min incubation—either in light (PPFD $600 \, \mu mol \, m^{-2} \, s^{-1}$) for net photosynthesis measurements or in complete darkness for respiration measurements. During dark measurements, all handling was conducted under green light (PPFD $<15 \, \mu mol \, m^{-2} \, s^{-1}$; Figure S4). All measurements were conducted using a Delta Ray Isotope Ratio Infrared Spectrometer TMURI (Thermo Fisher Scientific, Bremen, Germany; Qtegra™ ISDS 2.3.1487.49 software) and the data are available online (Witzgall et al., 2024).

The output from the spectrometer ($\mu mol \, CO_2 \, mol^{-1}$) was converted to $\mu mol \, CO_2$ with the ideal gas law, from which photosynthesis and respiration fluxes were calculated as

$$CO_2 \, flux = \frac{CO_{2_{headspace}} - CO_{2_{flush}}}{A \times t}$$

with CO_2 flux: net ecosystem exchange of CO_2 (in $\mu mol \, m^{-2} \, s^{-1}$); $CO_{2 \, headspace}$: CO_2 content in the headspace after incubation (in μmol); $CO_{2 \, flush}$: CO_2 content before incubation (here: ~16.8 μmol); A: surface area of sample (in m^2); and t: time of incubation (in s).

The photosynthesis data presented in this study represent the net CO_2 uptake (gross photosynthesis subtracted by respiration), that is, the net ecosystem exchange (NEE) of the entire biocrust–soil system and will be referred to as net photosynthesis hereafter. The gas measurements were conducted after 60 days of drought (10 days prior to harvest). The gas measurements and sampling system are described in detail in Witzgall et al. (2023).

2.5 | VNIR hyperspectral imaging

Hyperspectral imagery was used to estimate biocrust cover of each microcosm. All cores were gently sprayed with water, and after 30 min, images of the moist soil surfaces were recorded with a Hyspex VNIR-1800 camera (Norsk Elektro Optikk, Oslo, Norway) after automatic dark background correction. The sensor was equipped with a 30-cm lens, giving a field of view of approximately 9 cm ($53 \times 53 \, \mu m^2$ per pixel). Light reflectance intensity was measured for 186 bands (400–990 nm; spectral resolution of 3.17 nm per band). To account for potential unevenness in spectral response of the sample at different locations, the spectral intensity (I) was normalized to a 50% reflectance (R) calibration target for each wavelength (λ) and pixel (x)

$$R_{Sample, \lambda, x} = \frac{I_{Sample, \lambda, x}}{I_{Target, \lambda, x}} \times R_{Target, \lambda, x}.$$

A standard circle was cropped from each sample (1,537,844 pixels, total area of 43.2 cm^2). Regions of interest were selected where bryophytes, microbial biocrust, or bare soil without any biocrust cover were visible, and the spectral signatures were isolated for each of the three groups (Figure S7). Based on distinct differences in the spectral signatures between the groups, a set of ratios and associated thresholds were established in order to classify the pixels into two general types of biocrusts—bryophytes and general biocrust. Pixels were classified as bryophytes if the normalized difference vegetation index (NDVI) was ≥0.33, the sum of the RGB band's reflectance was >5, the ratio of bands 87/48 (680.9/556.7 nm) was <0.9, and the ratio of bands 60/50 (594.9/563.1 nm) was <1.1. The NDVI (Kriegler et al., 1969) was calculated as

$$NDVI = \frac{R_{NIR} - R_{RED}}{R_{NIR} + R_{RED}},$$

where R_{NIR} and R_{RED} are the reflectance of the near infrared (849.7–881.5 nm) and red (636.3–674.5 nm) bands. Pixels that did not meet the criteria for bryophytes were classified as general biocrusts if the sum of RGB band's reflectance was >5, the ratio of bands 87/77 (680.9/649.0 nm) was <0.95, and the ratio of bands 60/50 (594.9/563.1 nm) was ≥1.1. A detailed description of the thresholds and the classification approach is included in supplements (Figures S7–S11). The sum of pixels associated with bryophytes and general biocrusts is referred to as total biocrust cover hereafter.

2.6 | Sampling after incubation

After 133 days, mesocosms were harvested and separated into three depth increments. The biocrust layer was separated by lifting off the aggregated surface layer, including the soil adhering to it from below (Figure S6). The surface of the remaining soil in the cylinder was scraped off to collect all residues of the biocrusts and added to the biocrust layer. The same was done for the bare soil, where a similar amount of soil was gently separated to serve as a control for the biocrust layer. The uppermost soil layer (1 cm) of pure soil was then collected down to the Teflon foil, followed by the sublayer (subsequent 1.5 cm). These are hereafter referred to as 0–1 cm and 1–2.5 cm soil layers. Replicates were pooled by two to minimize the effect of natural heterogeneity between samples, that is, the eight incubation replicates resulted in four replicates for subsequent analyses. Samples for microbial analyses (PLFA) were freeze-dried immediately after sampling and stored at −20°C until analysis, while subsamples for elemental analyses (C, N, ^{13}C, and ^{15}N) and fractionation were air-dried in darkness at room temperature.

2.7 | Physical fractionation and subsequent analyses

Air-dried soil (20 and 25 g for biocrust and top layer, respectively) was capillary saturated with sodium polytungstate solution ($Na_6[H_2W_{12}O_{40}]$; $1.8\,g\,cm^{-3}$) overnight. After ultrasonic dispersion ($440\,J\,mL^{-1}$; Amelung & Zech, 1999; Mueller et al., 2014), floating particulate organic matter (POM) at the surface was separated from heavier minerals using a vacuum pump. The remaining mineral material was sieved ($63\,\mu m$) yielding two mineral-associated OM fractions ($MAOM_{<63\mu m}$ and $MAOM_{>63\mu m}$ hereafter). All fractions were washed with deionized water and pressure filtered ($0.22\,\mu m$) below an electrical conductivity of $<5\,\mu S\,cm^{-1}$. The fractions were freeze-dried and milled, after which the C, N, ^{13}C, and ^{15}N contents were determined by dry combustion with an isotope ratio mass spectrometer (Delta V Advantage, Thermo Fisher Scientific, Bremen, Germany) coupled to an elemental analyzer (Euro EA, Eurovector, Milan, Italy). Acetanilide was used as a laboratory standard for calibration and to determine the isotope linearity of the system. Several suitable isotope standards were further used for internal calibration (International Atomic Energy Agency, Vienna, Austria). The presence of $CaCO_3$ could be excluded as the elemental composition of samples treated with 0.5 M HCl remained identical to those without added HCl. Therefore, the total C content was assumed to be equal to the organic C content in subsequent measurements.

2.8 | Calculations of biocrust-derived C and N in bulk soil and OM fractions

The atom% of ^{13}C and ^{15}N in each sample, derived from the isotopic signatures $\delta^{13}C‰$ V-PDB and $\delta^{15}N‰$ air N_2, was used to calculate the adjusted molar mass of C and N (adapted from Teixeira et al., 2023):

$$M_C\,[g\,mol^{-1}] = \left(M_{13C} \times \frac{^{13}C_{atom\%}}{100}\right) + \left(M_{12C} \times \left(1 - \frac{^{13}C_{atom\%}}{100}\right)\right),$$

$$M_N\,[g\,mol^{-1}] = \left(M_{15N} \times \frac{^{15}N_{atom\%}}{100}\right) + \left(M_{14N} \times \left(1 - \frac{^{15}N_{atom\%}}{100}\right)\right),$$

where M_C and M_N are the adjusted molar mass for C and N, respectively, taking the isotopic enrichment of each sample into account. The molar mass of ^{13}C (M_{13C}) was set at 13.00335, that of ^{12}C (M_{12C}) at 12, that of ^{15}N (M_{15N}) at 15.000109, and that of ^{14}N (M_{14N}) at $14.003074\,g\,mol^{-1}$.

Furthermore, to account for the natural abundance of the stable isotopes, the excess isotopic enrichment of ^{13}C and ^{15}N was calculated:

$$^{13}C\,enrichment[\%] = {}^{13}C\,atom\%\,biocrust - {}^{13}C\,atom\%\,bare\,soil.$$

$$^{15}N\,enrichment[\%] = {}^{15}N\,atom\%\,biocrust - {}^{15}N\,atom\%\,bare\,soil.$$

Lastly, the excess content of ^{13}C and ^{15}N was determined (Teixeira et al., 2023):

$$^{13}C_{concentration}\,[\mu g\,g^{-1}] = \frac{^{13}C}{C}\,enrichment\%\,100 \times C_{soil} \times \frac{M_{13C}}{M_C} \times 1000,$$

$$^{15}N_{concentration}\,[\mu g\,g^{-1}] = \frac{^{15}N}{N}\,enrichment\%\,100 \times N_{soil} \times \frac{M_{15N}}{M_N} \times 1000,$$

where C_{soil} and N_{soil} are the total C and N contents in bulk soil or OM fractions.

2.9 | PLFA analyses

Phospholipid fatty acid patterns were determined according to Quideau et al. (2016), where lipids were extracted from freeze-dried soil (5 and 6 g for biocrust and top layer, respectively) using a Bligh and Dyer solution [methanol, chloroform, citrate buffer (pH=4), 2:1:0.8, v/v/v]. Each sample was spiked with C19:0 phosphatidylcholine dissolved in chloroform (Avanti Polar Lipids, Birmingham, UK) as an internal standard and stirred overnight at room temperature. Phases were separated by addition of chloroform and a citrate buffer, from which the lipid phase was collected and evaporated to dryness at 30°C under a stream of N_2. Neutral lipids and glycolipids were discarded by solid-phase extraction on silica tubes (SPE DSC-Si, 500 mg, Discovery®, Sigma-Aldrich, Taufkirchen, Germany), leaving phospholipids to be eluted, and the solvent (methanol) to be evaporated, before converting them to fatty acid methyl esters (FAMEs) by alkaline methanolysis. FAMEs were quantified by gas chromatographic analysis using retention times to identify the different compounds based on comparison with known analytical standards with a Perkin Elmer 8700 Gas Chromatograph equipped with a capillary column (Supelcowax 10™ 30 m × 0.53 mm, 2 μm coating, Sigma-Aldrich, Taufkirchen, Germany). The FAMEs used for quantification of gram+ bacteria were iC15:0, aC15:0, iC16:0, iC17:0, C17:0; gram−: C16:1ω7; fungi: C18:2ω6,9, C20:5ω3; actinomycetes: 10MeC16:0, 10MeC17:0, 10MeC18:0; cyanobacteria: 20:3ω3; bacteria: C15:0, aC17:0, cy19:0, and unspecified microorganisms: C14:0, C18:0, C20:0. All FAMEs were quantified relative to the internal standard:

$$C_{FA}\,[nmol\,g^{-1}] = \frac{\frac{area\,count_{FAME} \cdot C_{C19:0}}{area\,count_{C19:0}}}{g},$$

where area $count_{sample}$ is the integrated signal of a peak of a given FAME, $C_{C19:0}$ is the amount of C-C19:0 atoms added at spiking (in nmol), area $count_{C19:0}$ is the integrated signal of the internal standard peak, and g the amount of soil used for extraction.

The isotopic enrichment of different FAMEs was analyzed using a Rtc-5 60 m/0.25 mmID/1 μm coated column (Restek, Bellefonte, PA, United States) coupled to a Delta V Advantage mass spectrometer via GC Isolink (Thermo Fisher Scientific, Bremen, Germany). This instrumentation allowed online conversion of all FAMEs in the

eluate from the GC column directly to CO_2 and continuous measurement of the ^{13}C to ^{12}C ratios in the He (carrier gas)-CO_2 stream that was subsequently fed to the mass spectrometer (López-Mondéjar et al., 2018). The identification of different fatty acids was achieved by comparing their retention times with qualitative GC standards. The excess ^{13}C isotope enrichment was then calculated for each of the individual FAMEs:

$$^{13}C_{enrichment}[\%] \text{ in FAME} = {}^{13}C_{atom}\%\, biocrust - \overline{{}^{13}C_{atom}\%\, baseline},$$

where $^{13}C_{atom\%\ baseline}$ is the average atom% in baseline samples prior to incubation, representing the natural abundance levels in each FAME prior to labeling.

2.10 | Statistical analyses

Data were analyzed using R (version 4.2.1) in R studio (version RStudio 2022.07.2+576; R Studio Team, 2015). The CO_2 flux data were tested with an ANOVA with the treatments (ambient vs. warming) and drought (normal water vs. drought) as fixed effects for the samples with biocrusts only. The elemental composition of the layers and OM fractions was tested for differences using a mixed effect model (lme, package: nlme version: 3.1-157; Pinheiro et al., 2024) with the treatment, drought and biocrust (yes vs. no) as fixed effects and the ID of each sample as a random effect. The PLFA data were also tested with an lme with treatment, drought, and the depth (biocrust vs. top layer) as fixed effects and the ID as a random effect. For all models, post hoc tests were performed with the Tukey method for the desired comparisons between single groups. For ANOVA, the Tukey test was applied and for lme the emmeans test (package: emmeans version: 1.8.8; Lenth, 2023). Normality of the residuals (Shapiro test/qq-plots) and homogeneity of variances (Levene test, package: car, version: 3.1-2) were tested for every model beforehand, and data were log-transformed if necessary. Correlations between single parameters were done with the chart.correlation function (package: PerformanceAnalytics, version: 2.0.4; Peterson & Carl, 2020) using the Spearman's method. All errors in the text and graphics refer to the standard deviation of the mean (SD).

3 | RESULTS

3.1 | Changes in CO_2 fluxes and biocrust functionality due to drought and warming

The CO_2 flux measurements revealed distinct effects of biocrusts, temperature, and drought on dark respiration and net photosynthetic CO_2 assimilation. Respiration was significantly higher in all biocrust systems compared to the corresponding bare soil controls ($p \leq .005$ in all cases), highest in biocrusts exposed to warming and no drought ($0.36 \pm 0.11\,\mu mol\ CO_2\ m^{-2}\ s^{-1}$; Figure 1). Warming accelerated respiration, particularly under normal water conditions (by a factor of ~2; $p = .001$). Respiration

was inhibited by drought, most pronounced in systems exposed to warming (by a factor of ~−2; $p \leq .001$). Similar patterns were observed for photosynthesis measurements, where drought strongly constrained photosynthetic assimilation of CO_2 both at ambient temperature (from 0.21 ± 0.13 to $0.05 \pm 0.03\,\mu mol\ CO_2\ m^{-2}\ s^{-1}$; $p = .002$) and under warming (from 0.24 ± 0.10 to $0.03 \pm 0.05\,\mu mol\ CO_2\ m^{-2}\ s^{-1}$; $p \leq .001$; Figure 1). Overall, net photosynthesis and respiration rates were strongly correlated across biocrust systems ($\rho = .80$; $p = .001$) and all proxies for biocrust cover were positively correlated with photosynthesis ($\rho > .51$; $p < .001$ in all cases) and respiration ($\rho > .71$; $p < .001$ in all cases; Table S4). No photosynthesis was measured in bare soil controls.

Overall, biocrust surface cover increased with warming, reaching as high as $38.26 \pm 8.97\%$ compared to $19.35 \pm 10.90\%$ in systems at ambient temperature ($p = .003$; Table S3). When CO_2 fluxes were normalized by biocrust surface cover to assess biocrust functionality, expressed in $\mu mol\ CO_2\ m^{-2}$ biocrust s^{-1}, the photosynthetic uptake was no longer only affected by drought (still significant in all cases; $p \leq .001$), but also showed a strong effect of temperature (Figure 1b); warming decreased the CO_2 uptake almost by half in normal-watered systems (from 1.23 ± 0.29 to $0.72 \pm 0.18\,\mu mol\ CO_2\ m^{-2}$ biocrust s^{-1}; $p = .0011$; Figure 1b; Figure S13).

3.2 | Evidence of biocrust-derived C translocated into deeper soil layers under ambient temperatures

Bulk C and N contents were clearly elevated in the biocrust layer compared to the corresponding bare soil controls (Figure 2; $p \leq .01$ in all cases), with the highest contents observed in normal-watered biocrusts. While warming did not affect bulk contents in the biocrust layer, we determined temperature effects in the underlying 0–1 cm soil. Here, bulk C contents were elevated under biocrusts compared to controls at ambient temperature under normal-watered (4.59 ± 0.21 vs. $4.09 \pm 0.21\,mg\ C\ g^{-1}$ in bare soils; $p = .033$) and drought conditions (4.48 ± 0.34 vs. $3.95 \pm 0.15\,mg\ C\ g^{-1}$ in bare soils; $p = .025$). This distinction that was not reflected in biocrusts systems exposed to warming, where C contents instead remained similar to bare soil controls. The N contents followed identical patterns (Figure 2).

3.3 | Contrasting effects of artificial warming on C and N fixation

The distribution of biocrust-derived ^{13}C in the bulk soil followed similar patterns as the bulk C data. We found the excess ^{13}C content in the biocrust layer to decrease only slightly due to drought, from 47.44 ± 23.39 to $26.06 \pm 6.00\,\mu mol\ ^{13}C\ g^{-1}$ at ambient temperature ($p = .129$) and from 66.94 ± 17.86 to $47.55 \pm 11.55\,\mu mol\ ^{13}C\ g^{-1}$ under warming ($p = .165$; Figure 3). Interestingly, the patterns in biocrust-derived ^{15}N were different. Here, excess ^{15}N remained unchanged between moisture levels at ambient temperature ($0.24\,\mu g\ ^{15}N\ g^{-1}$ in both), whereas
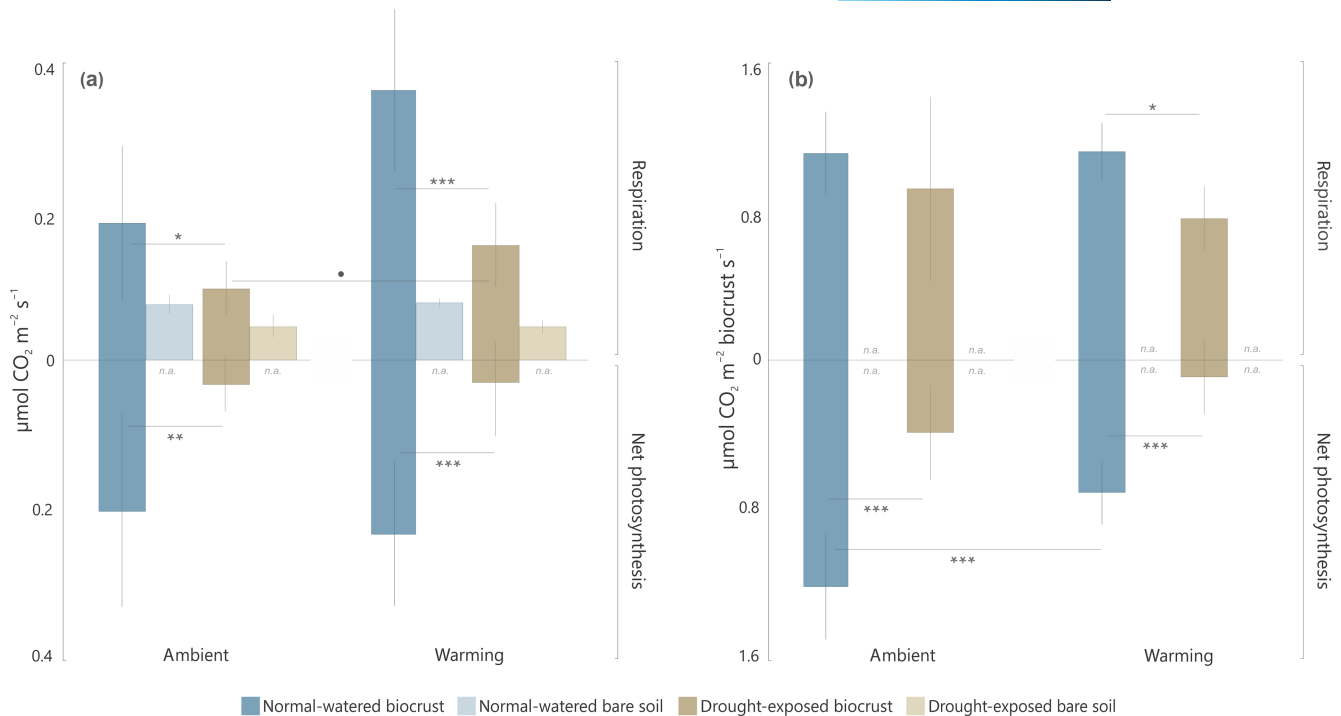
FIGURE 1 (a) Respiration and net photosynthesis (μmol CO_2 m^{-2}s^{-1}) in soils with biocrusts (bold colors) or without (faded colors), either under normal water conditions (blue) or drought (brown) and at "ambient" temperatures (corresponding to field conditions) or under experimental warming (+5°C). The net photosynthesis reported here represents the total CO_2 flux of the biocrust–soil system and is therefore equivalent to net ecosystem exchange. If net photosynthesis is greater than zero, this equates to a net C gain in the system. Photosynthesis could be excluded in bare soils ("n.a."). Bars represent means, SDs displayed with error bars, $n=8$ independent replicates. (b) Respiration and net photosynthesis as a function of biocrust surface cover (μmol CO_2 m^{-2} biocrust s^{-1}) only in biocrust systems, as there was no biocrust cover in bare soils (means, SDs displayed with error bars, $n=8$ independent replicates). Asterisks denote significant differences between ambient and warming, and between the normal water and drought treatment ($^{\bullet}p<.1$, $^{*}p<.05$, $^{**}p<.01$, $^{***}p<.001$). Respiration rates were higher in all biocrusts compared to bare soils ($p \le .005$ in all cases) and are not indicated in the figure.

warming combined with drought induced a decrease (from 0.27 ± 0.09 to $0.17\pm0.02\mu$g ^{15}N g^{-1}; $p=.084$; Figure 3). We found diverging correlation patterns between ^{13}C and ^{15}N contents in the crust layer. For example, while ^{13}C was positively correlated with all proxies for biocrust cover ($\rho\geq0.63$, $p\leq0.0001$), respiration ($\rho=.71$, $p\leq.001$), and photosynthesis ($\rho=.49$, $p=.005$), there was no correlation for ^{15}N (Table S4).

The isotopic composition of the underlying soil layers showed similar contents of biocrust-derived C in the 0–1 cm soil layer regardless of temperature scenario. Similar to the ^{13}C patterns observed in the biocrust layer, drought was the limiting factor for downward translocation of C from the biocrusts into the soil (Figures S15 and S16). The ^{13}C content in the underlying soil layer was strongly correlated to both respiration and photosynthesis rates ($\rho=.76$, $p \le .001$, respectively, $\rho=.80$, $p=.002$) as well as to biocrust cover, most particularly to moss cover ($\rho=.70$, $p \le .001$).

3.4 | Formation of particulate and mineral-associated OM within and below biocrusts

The allocation of OM within specific OM pools was assessed by soil fractionation according to density and size. We found a clear build-up of C within the smaller mineral-associated fraction (MAOM$_{<63\mu m}$)

in the biocrust layer across temperature and moisture treatments, ranging from 3.52 to 3.98 mg C g^{-1} in biocrusts compared to 1.81–2.24 mg C g^{-1} in corresponding bare soil controls ($p \le .001$ in all cases; Figure 4). Although not significant, C allocated as POM in biocrusts under ambient conditions was slightly elevated (2.68 ± 1.41 compared to 1.60 ± 0.05 mg C g^{-1} in the bare soil controls; $p=.159$). This pattern was reversed in biocrusts under drought and warming, where the POM fraction was instead slightly C depleted compared to in the bare soil ($p=.119$). In the underlying soil layer, warming and drought resulted in C depleted POM (1.72 ± 0.07 under biocrusts compared to 1.92 ± 0.04 mg C g^{-1} in the bare soils; $p=.026$). The most striking difference in the subsurface soil was found in MAOM$_{<63\mu m}$ under ambient temperature and watering, which was the only fraction with elevated C content under biocrusts compared to controls (2.12 ± 0.14 compared to 1.74 ± 0.16 mg C g^{-1}; $p=.090$). The N contents across the OM fractions followed the same pattern as C (Figure S17).

3.5 | Microbial community shift under biocrusts

Changes in microbial community structures under biocrusts were captured by microbial-derived PLFA profiles. Microbial abundance was strongly enhanced in biocrust layers compared
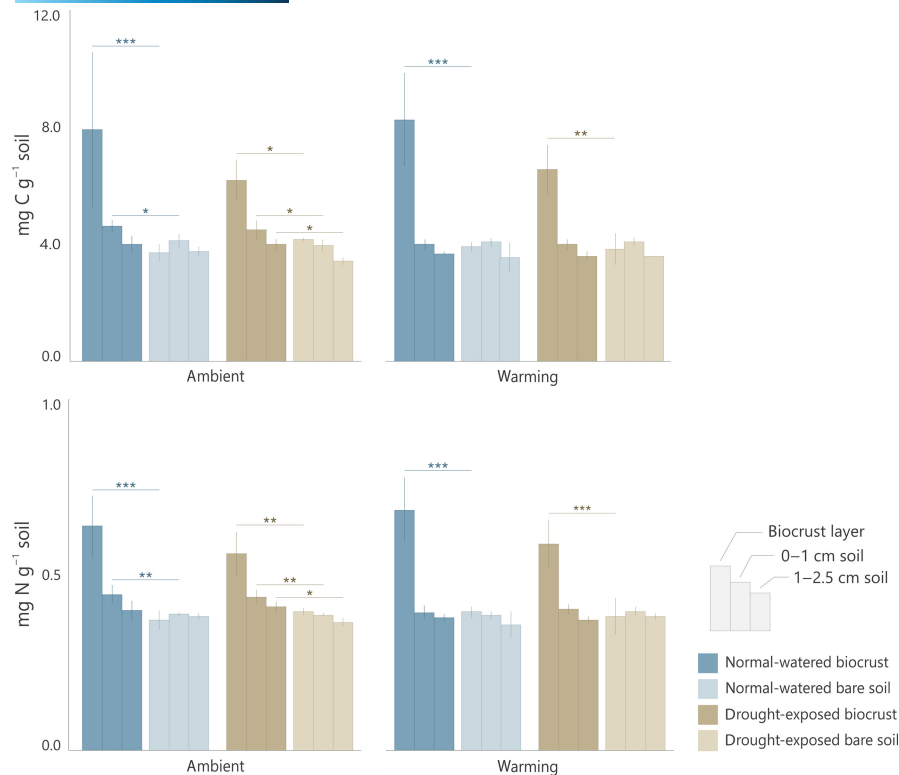
FIGURE 2 C and N contents (mg g^{-1} soil) across three depth increments; biocrust layer and underlying top (0–1 cm) and sub (1–2.5 cm) soil layers in biocrust samples (bold colors) and bare soils (faded colors), either under normal water conditions (blue) or drought (brown). "Ambient" represents temperatures corresponding to field conditions and "warming" +5°C throughout the incubation (means, SDs displayed with error bars, $n = 3$ independent replicates). Asterisks denote significant differences between biocrusts and their corresponding bare soil controls (*$p < .05$, **$p < .01$, ***$p < .001$).

to bare soils ($p \leq 0.003$ in all cases), with slightly higher abundance in normal watered biocrusts compared to drought. Overall, increased microbial abundance in biocrusts was associated with increased dominance of fungi (reflected by higher fungi: bacteria ratios; Figure 5c) and a relative increase in gram– bacteria (reflected by lower gram+:gram– ratios; Figure 5e). The fungi:bacteria ratio was positively correlated with C ($\rho = .82$, $p < .001$), N ($\rho = .80$; $p < .001$), and ^{13}C ($\rho = .93$, $p < .001$) contents in the biocrust layer, but also with the ^{13}C content in the underlying soil ($\rho = .88$, $p < .001$). Furthermore, we found a correlation between fungi:bacteria ratio and biocrust cover ($\rho = .63$, $p < .001$; Table S5). Neither of these correlations were true in any of the other microbial proxies.

In the underlying soil, we detected changes in microbial community composition due to warming. The relative dominance of fungi was the highest under ambient conditions (1.21 ± 0.38 vs. 0.28 ± 0.04 in the corresponding bare soil control; $p = .002$) compared to warming, where instead the absolute abundance of bacteria was elevated (Figure S22). We found a strong correlation between fungi: bacteria ratio in the underlying soil layer and C and N contents of the MAOM$_{<63\mu m}$ fraction ($\rho = .72$, $p = .001$ in both cases), which was not reflected in any other parameters.

Total microbial uptake of biocrust-derived C, quantified by ^{13}C-PLFA profiles, was clearly enhanced by warming (1.49 ± 0.35 compared to 0.59 ± 0.21 µg ^{13}C g^{-1} under ambient

conditions; $p \leq .001$; Figure 6). Regardless of temperature, drought reduced the microbially assimilated ^{13}C by half ($p = .175$ in ambient temperature and $p = .002$ under warming). The distribution of ^{13}C among microbial groups showed the highest allocation of ^{13}C in fungal biomass, with a >75% contribution of fungal markers (Figure 6). The assimilation of ^{13}C into microbial biomass in both biocrust layer and underlying soil was positively correlated with biocrust cover, respiration and photosynthesis (Table S5). Interestingly, the latter was only weakly correlated with microbial ^{13}C in the biocrust layer ($\rho = .44$, $p = .038$) but strongly correlated in the underlying soil ($\rho = .81$, $p \leq .001$).

4 | DISCUSSION

In this study, we trace pathways of biologically fixed C and N from biocrusts, via microbial transformation, into the underlying mineral soil. Our main objective was to improve the understanding of the ecological consequences of climate change on fundamental biogeochemical cycles in dryland ecosystems at the process level. We used a systems approach to directly link biocrusts—as key dryland primary producers—with the fate of recently fixed C and N in SOM pools. Specifically, dual ^{13}CO$_2$ and ^{15}N$_2$ labeling allowed detailed tracing of elemental pathways into
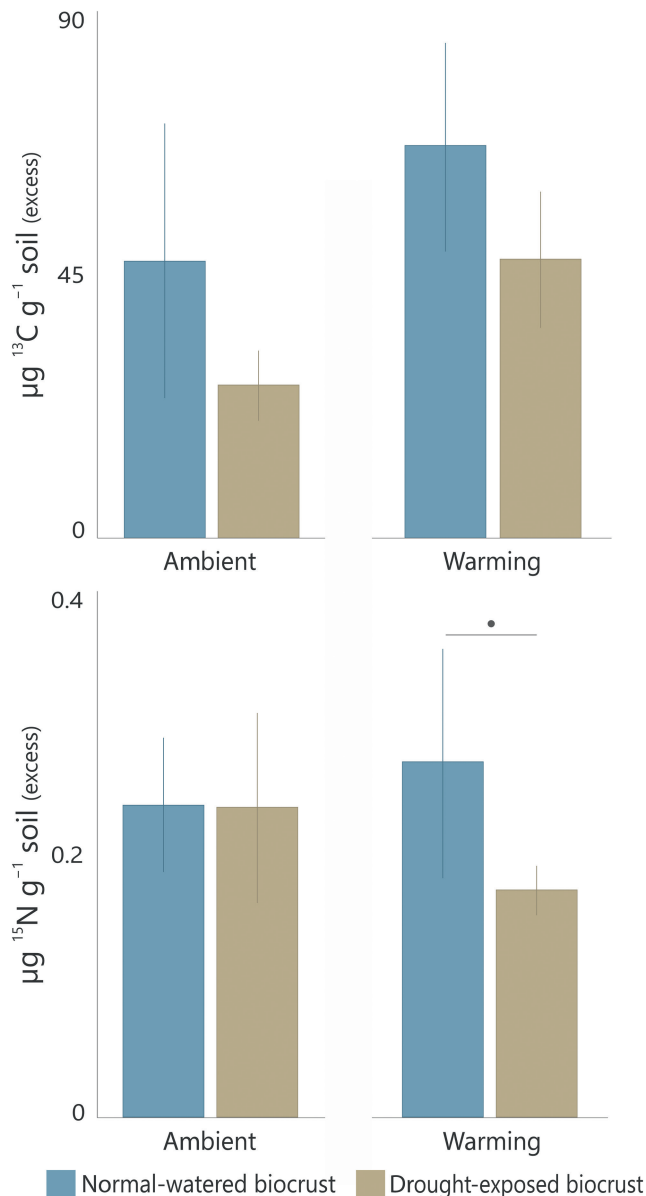
FIGURE 3 Biocrust-derived ^{13}C and ^{15}N ($\mu g\,g^{-1}$) within the biocrust layer (excess, corrected by isotopic composition of bare soil controls) under normal-watered (blue) and drought (brown) conditions. "Ambient" represents temperatures corresponding to field conditions and "warming" $+5°C$ throughout the incubation (means, SDs displayed with errors bars, $n=3$ independent replicates). The bullet point denotes a weakly significant difference between normal-watered and drought-exposed biocrusts ($•p < .1$).

specific OM fractions and into microbial biomass in a controlled phytotron incubation setup; a setup which, to our knowledge, has not previously been implemented in soil–biocrust systems. This not only provided novel insights into the contribution of biocrusts to soil C and MAOM formation in the subcrust soil at the mechanistic level but also showed how changing climatic conditions offset fundamental biogeochemical pathways into the mineral soil, with possible consequences for the overall C balance of the system.

4.1 | Warming and drought effects on C fluxes and biocrust functionality

We successfully quantified photosynthetic C uptake and enhanced respiration in all biocrust systems compared to bare soils, confirming the key role of biocrusts as regulators of C fixation and release in drylands (Figure 1a; Castillo-Monroy et al., 2011; Dacal et al., 2020). Photosynthesis and respiration were positively correlated (Table S4), underscoring the interdependence between soil heterotrophs and the primary production of biocrust autotrophs (Tucker et al., 2020). This was also confirmed by both photosynthesis and respiration being positively correlated with all proxies for biocrust cover quantified by hyperspectral imaging (Table S4), emphasizing how biocrusts modulate soil respiration via the intricate association to soil heterotrophs (Castillo-Monroy et al., 2011; Dacal et al., 2019). Only at optimal water availability, biocrust systems exhibited an overall net C gain, with photosynthetic uptake exceeding respiratory losses regardless of temperature (up to $>0.4\,\mu mol\,CO_2\,m^{-2}\,s^{-1}$ net C uptake in systems with the highest biocrust cover; Figure 1a). These rates either align or fall within the lower end of field trials in which net ecosystem exchange fluxes were quantified at $\sim0.5–2\,\mu mol\,CO_2\,m^{-2}\,s^{-1}$ in similar dryland ecosystems (Bowling et al., 2011; Darrouzet-Nardi et al., 2015). We attribute the lower fixation rates in this study to the short time frame of the experiment (~4.5 months) in relation to biocrust growth and development rates (Weber et al., 2016).

Our results further underscore the well-established concept of moisture availability as a primary constraint on C fluxes in drylands, where heterotrophic and photosynthetic activity are typically confined to brief hydration events between prolonged periods of desiccation (Bowling et al., 2011; Coe et al., 2012; Lange, 2001). In the present study, drought was clearly the dominating factor constraining CO_2 fluxes, reducing photosynthetic C uptake by $>80\%$ to the point where the C balance was verging on net negative in biocrust systems exposed to drought—despite lower respiratory C losses. Our data suggest that even short-term drought exposure limits the ability of biocrusts to sustain metabolism to an extent that counteracts their contribution to a positive C balance in these dryland systems.

We found respiration to increase in biocrusts exposed to warming (Figure 1a), which we attribute to accelerated C turnover, likely due to increased kinetic energy of enzymes and diffusion rates at elevated temperatures (Davidson et al., 2006; Tucker & Reed, 2016). However, no notable increase in microbial biomass was observed (Figure 5a), suggesting lower microbial C use efficiency in systems exposed to warming (i.e., a lower proportion of C incorporated into microbial biomass compared to the total C consumed). This may be ascribed to higher energy costs of maintaining existing microbial biomass under warmer conditions (Sinsabaugh et al., 2013; Tucker et al., 2013). Elevated respiration triggered by warming has been shown to revert to ambient levels over time along with the depletion of labile C resources or microbial adaptation (Bradford et al., 2008; Dacal et al., 2019; Darrouzet-Nardi et al., 2015; Eliasson et al., 2005; Tucker et al., 2013). This underlines the need for continuous C inputs from primary producers
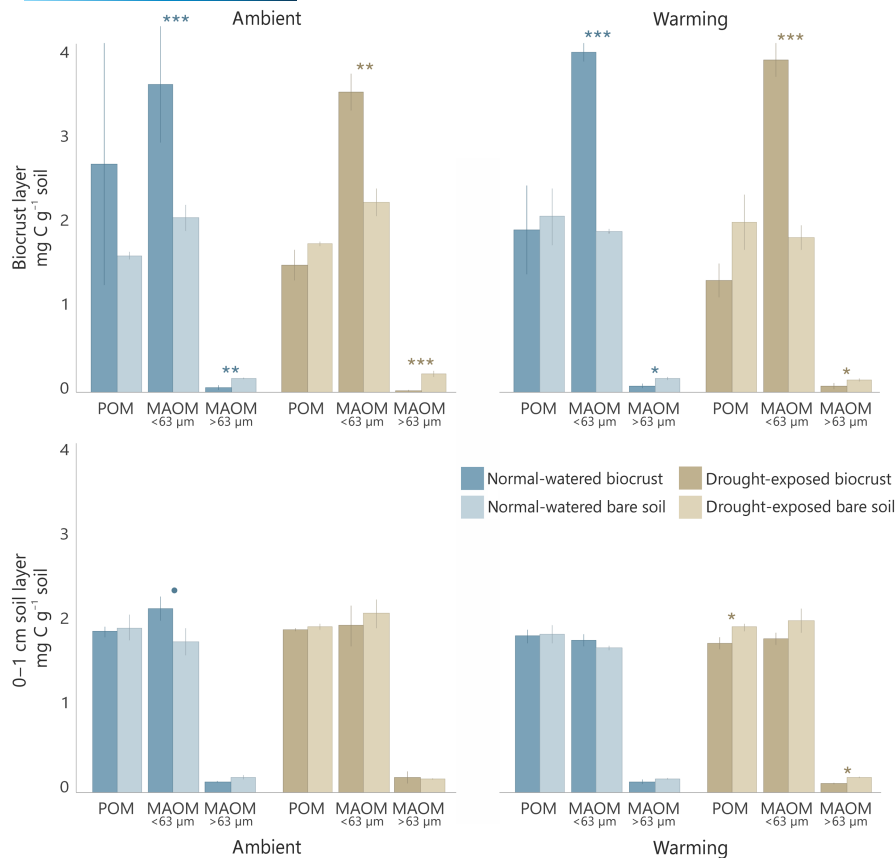
FIGURE 4 The C contents (in mg C g^{-1} soil) in the biocrust layer an underlying 0–1 cm soil layer within particulate (POM) and mineral-associated OM (MAOM$_{<63\mu m}$ and MAOM$_{>63\mu m}$) fractions. Bars represent means, SDs displayed with error bars, $n = 3$ independent replicates. Asterisks denote significant differences between biocrusts and their corresponding bare soil controls ($^{\bullet}p < .1$, $^{*}p < .05$, $^{**}p < .01$, $^{***}p < .001$).

in systems with accelerated microbial C consumption fueled by warming in order to sustain net C positivity over time. Overall, regardless of temperature, reduced moisture in the drought-affected biocrusts clearly dampened the respiratory response to warming, further suggesting a decreasing temperature sensitivity and an overriding influence of restricted soil moisture in the drought-exposed systems (Conant et al., 2004; Schimel, 2018).

Unlike respiration, net C uptake was demonstrated to be unaffected by warming. This was reflected in consistent bulk C (and N) contents in the biocrust layers regardless of the temperature regime (Figure 2). This nicely corroborates the direct connection between C fluxes from the biocrust systems and the subsequent build-up of C and N stocks within biocrust biomass. The fact that net C uptake could be maintained under warming, despite accelerated respiratory C losses, can be ascribed to overall higher gross photosynthesis, likely due to the greater soil surface coverage of biocrusts in the warmer chamber (Table S3). Consequently, the measured C fluxes unravel how temperature differences drive the development of two systems, each exhibiting a distinct dynamic. The system under warming is characterized by greater C gains and losses, accelerated by microbial C turnover. The increased throughput of C from the photoautotrophs was further reflected in slightly elevated content of biocrust-derived ^{13}C (not statistically significant; Figure 3) along

with distinctively higher ^{13}C in microbial biomass under warming, indicating an amplified microbial involvement in the processing of biocrust-derived C.

In the present study, biocrusts were allowed to develop naturally across the surface of the mesocosms, resulting in variable and heterogeneous soil surface coverage among the replicates (Table S3). To directly estimate warming and drought impacts on photosynthetic fluxes, C uptake was normalized to biocrust surface cover, serving as a proxy for biocrust functionality. When considering cover, warming was found to significantly restrict net C uptake (Figure 1b). Thus, while elevated temperature did not alter the total C balance in the systems, the data illustrate how warming impaired the capacity—or efficiency—of photoautotrophic components of the biocrust in fixing CO_2. This can be attributed to the more rapid desiccation under warming, resulting in shorter hydration periods of the biocrust and thereby preventing phototrophs from reaching their maximal fixation potential (Lange, 2001). The observed decrease in photosynthetic capacity and reduced biocrust functionality underscores the risk that biocrusts may no longer effectively withhold net photosynthetic C gain during prolonged exposure to warming (Darrouzet-Nardi et al., 2015; Maestre et al., 2013; Tucker et al., 2020) which could point to concerning implications for their capacity to function and sequester atmospheric CO_2 amid future global warming.
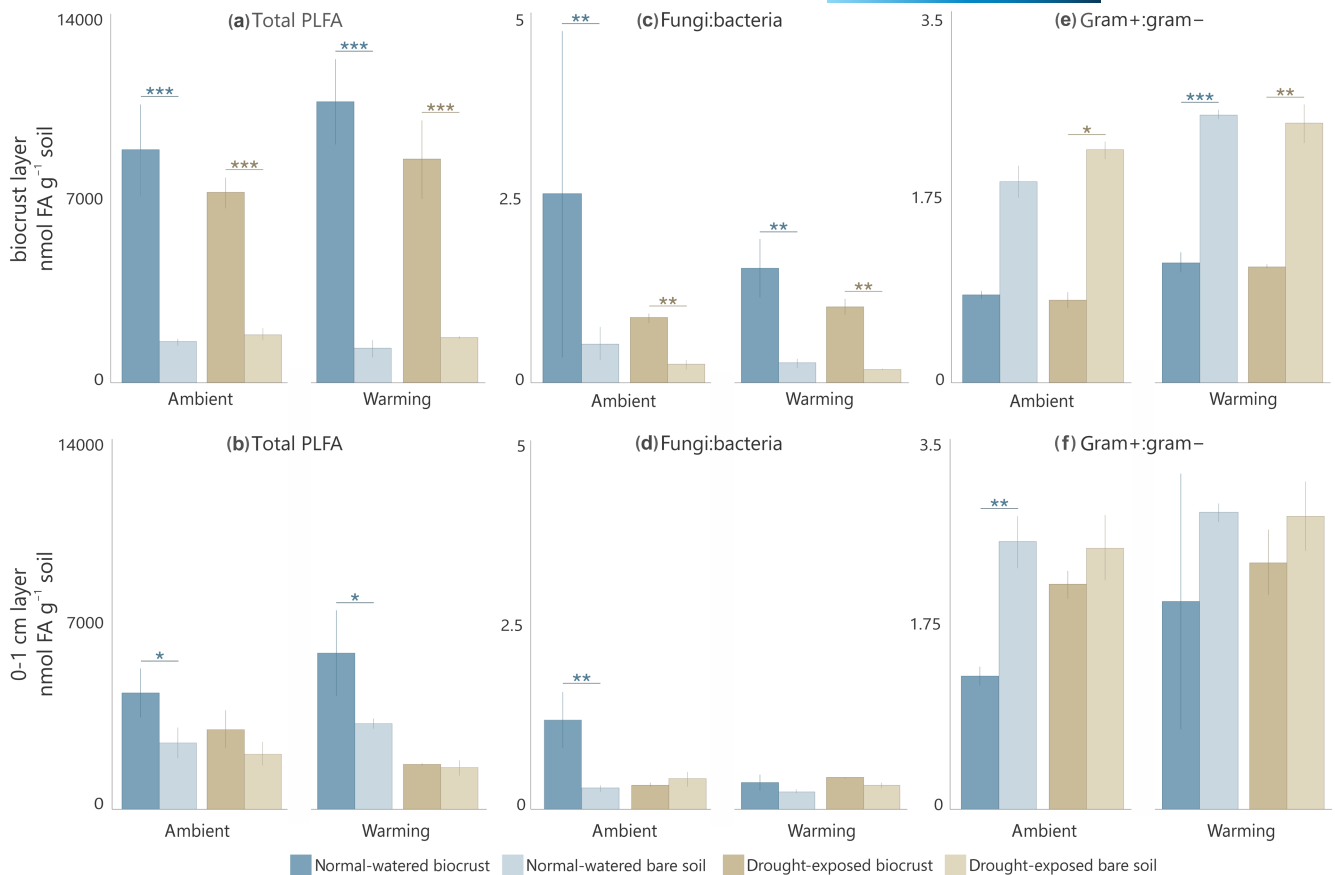
FIGURE 5 (a, b) Total abundance of phospholipid fatty acids (PLFA; in nmol FA g⁻¹), (c, d) fungi:bacteria ratio and (e, f) gram+:gram− ratio within the biocrust layer and the underlying 0–1 cm soil layer (means, SDs displayed with error bars, $n = 3$ independent replicates). Asterisks denote significant differences between biocrusts and their corresponding bare soil controls (*$p < .05$, **$p < .01$, ***$p < .001$).

4.2 | Warming and drought effects on biocrust C and N fixation and elemental pathways

The C flux patterns were directly reflected in the distinct accumulation of bulk C and N in the crust layers, emphasizing the major role of biocrusts in regulating C and N cycles in dryland ecosystems (Figure 2). This build-up of OM was consistent across all biocrust treatments and was associated with increased microbial biomass within the biocrusts, with only subtle effects of drought (Figure 5a). Specifically, the dominance of gram− bacteria (gram+:gram− ratios; Figure 5e) and fungi (fungi:bacteria ratios; Figure 5c) increased in all biocrusts. The overall increase in microbial biomass C underscores the contribution of biocrusts to alleviating soil nutrient scarcity, for example, through the release of bioavailable EPS (Mager & Thomas, 2011), and overall points to enhanced availability of labile and easily available C sources to stimulate microbial growth (Fanin et al., 2014; Kramer & Gleixner, 2008).

While the allocation of C and N in the biocrusts followed identical patterns overall, their isotopic composition did not, suggesting the processes involved in C and N fixation to be decoupled. In fact, there was no correlation between ¹³C and ¹⁵N contents within biocrusts (Table S4) and the isotopic patterns between the different biocrust treatments diverged; while ¹³C was slightly

enhanced under warming and showed similar drought effects between temperatures, recently fixed ¹⁵N displayed no drought effect at ambient temperature, while contents were lower in systems exposed to combined drought and warming (Figure 3). The interactive effect of drought and warming seems to limit the amount of atmospheric N entering the soil systems via biological N fixation. This is likely caused by the increased desiccation of biocrusts exposed to combined warming and drought, as moisture is generally known to be the primary environmental factor controlling N fixation (Barger et al., 2016; Rousk et al., 2018). Warming effects on N uptake has also been observed in long-term field trials, however, due to reducing cover of N-fixing biocrust under increasing temperatures (Finger-Higgens et al., 2022). Furthermore, warming has been demonstrated to accelerate oxidation of recently fixed ¹⁵N₂ by nitrifying bacteria (Johnson et al., 2005). Our results add to this, showing how reduced N fixation due to drought and warming is not directly linked to a decline in biocrust cover, but rather points to declined nitrogenase activity and overall functionality (Figure 1b) of the biocrust systems exposed to climatic change. As N is the main constraint to primary production after water in dryland ecosystems, altered N fixation potential of biocrusts can have major implications at ecosystem scales (Hooper & Johnson, 1999). Our results also nicely demonstrate the applicability of ¹⁵N₂ labeling
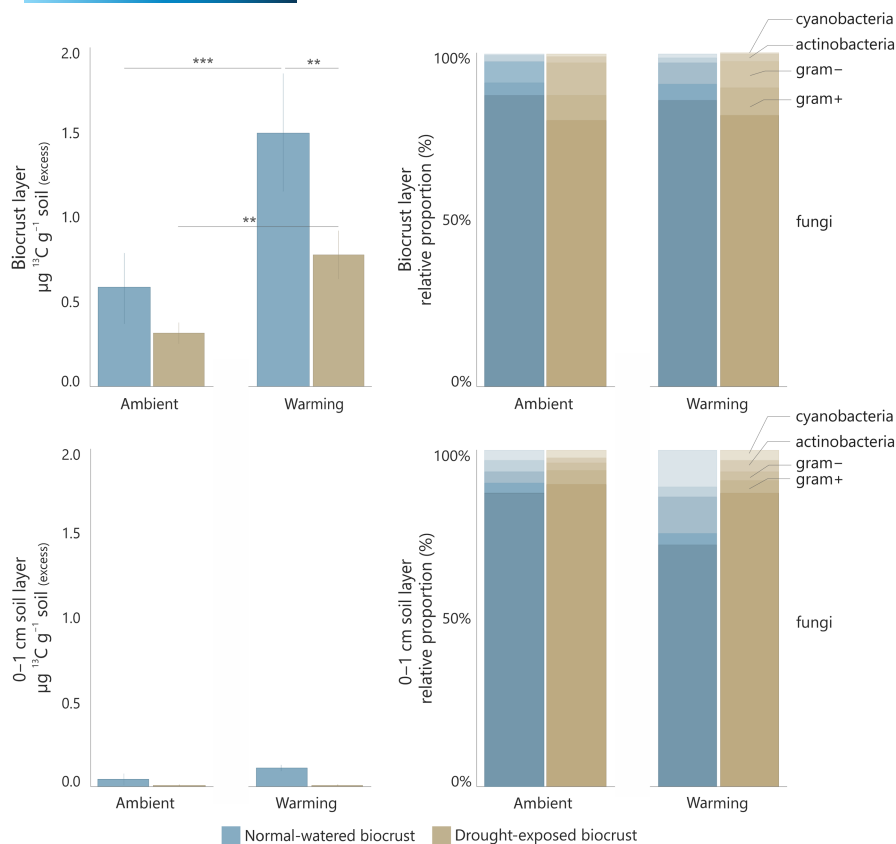
FIGURE 6 Total content of ^{13}C in microbial biomass (in μg ^{13}C g^{-1}) within the biocrust layer and the underlying 0–1 cm soil layer (excess, corrected by unlabeled samples; bars represent means, SDs displayed with error bars, $n=3$ independent replicates). The stacked bars show the distribution of the total ^{13}C content (in %) within microbial groups, from below: Fungi, gram+ bacteria, gram− bacteria, actinobacteria and cyanobacteria. Asterisks denote significant differences between biocrusts and their corresponding bare soil controls (**$p<.01$, ***$p<.001$).

to quantify the influence of drought and warming on short-term in situ N fixation in biocrusts, which to our knowledge have not been reported before.

4.3 | Allocation of C and N into POM and MAOM within biocrusts

The distinct build-up of C and N within the biocrust layer was mainly allocated into the mineral-associated OM fraction (MAOM$_{<63μm}$; Figure 4), highlighting the intricate connection between microorganisms and soil mineral particles as one of the key characteristics of biocrusts (Díaz-Martínez et al., 2023). The exact mechanisms involved in MAOM formation within biocrusts are largely unknown but are likely fostered by the filamentous growth of moss rhizoids and cyanobacterial filaments and bundles enmeshing soil minerals, creating biologically active biogeochemical interfaces and, thus, fostering MAOM formation (Mager & Thomas, 2011; Vidal et al., 2021; Weber et al., 2022; Witzgall et al., 2021). Additionally, increasing microbial necromass in the biocrust systems with stimulated microbial activity may further have contributed to MAOM (Angst et al., 2021).

Contrary to our expectations, we found no clear contribution of biocrusts to particulate OM (POM). In systems exposed to

warming and drought, POM was even slightly depleted in biocrusts and the underlying soil compared to in bare soils. We argue that this is caused by restricted growth and photosynthetic activity in biocrusts exposed to drought, and thereby reduced C inputs, while C losses via microbial mineralization were accelerated due to warming (Figure 1a). Over time, this depletion would progressively enhance resource limitations for microorganisms, leading to increased mineralization of remaining bioavailable C sources (POM; Schimel, 2018) which underscores the preferential loss of POM under warming (Link et al., 2003).

4.4 | C and N translocation from biocrust into the underlying soil

The elemental composition of the biocrust layers displayed no response to warming. Nonetheless, differences in C and N contents were notable in the underlying 0–1 cm mineral soil where C and N accumulated beneath biocrusts only in systems maintained at ambient temperature (Figure 2). Generally, processes such as increased infiltration due to channeling effect of moss stems and rhizoids (Kidron et al., 2010) or leaching of dissolved organic C (DOC) from biocrusts into the mineral soil (Young et al., 2022) can facilitate
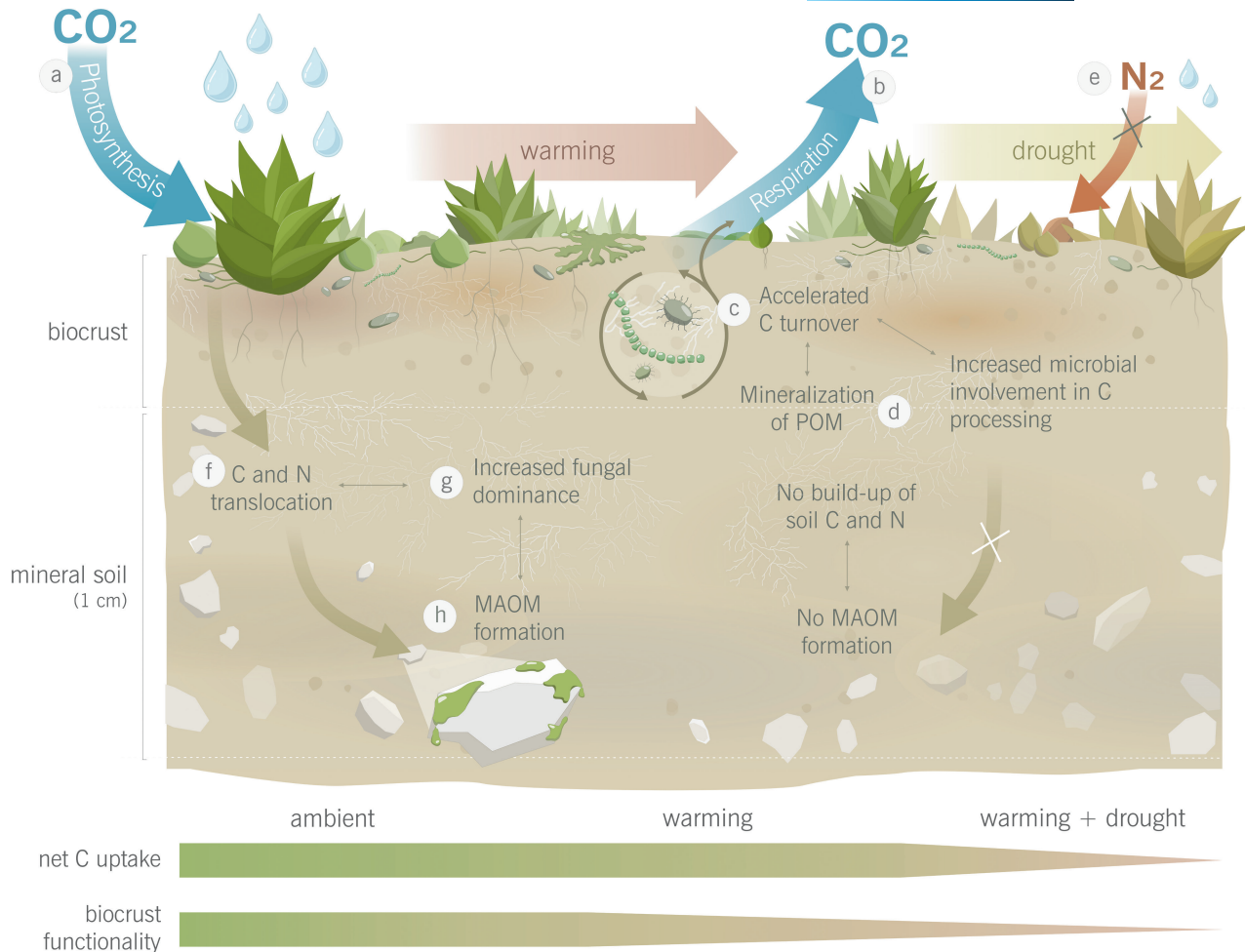
FIGURE 7 A conceptual overview of C and N pathways in biocrust–soil systems exposed to warming and drought. While net photosynthesis was not affected by temperature (a), respiration rates increased under warming (b), which was associated with accelerated C turnover (c). Elevated ^{13}C contents in microbial biomass under warming further indicated increased microbial involvement in processing of biocrust-derived C. In warming- and drought-affected systems, particulate OM was preferentially lost (POM; d) and net N fixation was hampered (e). In systems under ambient conditions, C and N was translocated from the biocrust into the underlying mineral soil (f), which was associated with increased fungal dominance (g) and the formation of mineral-associated OM (MAOM$_{<63\mu m}$; h) and. These processes were not reflected in systems exposed to warming.

downward C and N translocation from biocrusts. However, C and N levels in the warming-exposed soil beneath biocrusts remained consistent with bare soil controls (Figure 2), suggesting that mechanisms associated with downward C and N movement were inhibited—or offset—by elevated temperature. This may be due to the accelerated microbial turnover of biocrust-derived inputs in systems exposed to warming, as evidenced by increased respiration, resulting in a more rapid depletion of inpfacuts, thereby preventing downward C flow into the mineral soil. Moreover, increasingly disconnected soil pore spaces in a more rapidly drying soil under warming conditions may further contribute to C immobility, potentially restricting microbial access to C and microbial movement throughout the pore network (Smith et al., 2017). However, microbial immobility was not corroborated by the PLFA profiles. Instead, the content of biocrust-derived ^{13}C assimilated in microbial biomass was slightly higher in the soil beneath biocrusts exposed to warming (not significant; Figure 6). The elevated microbial ^{13}C contents thereby suggest an increased

involvement in the transformation of biocrust-derived compounds under warming.

Across all systems, fungi were prominently involved in C and N cycling, reflected in >75% of total microbial ^{13}C being allocated to fungal biomass (Figure 6). Furthermore, fungal abundance and fungi:bacteria ratio were the most prominent microbial variables that strongly correlated with several biogeochemical parameters (C, N, ^{13}C) in the biocrust layer (unlike the other microbial proxies; Table S5). The importance of fungi also extended into the subcrust soil, where the C and N accumulation under ambient conditions was associated with a distinct shift toward increased fungal dominance, similar to the shift in the biocrust layer (Figure 5). Our findings hereby emphasize the significance of fungal networks in drylands— from the biocrust into the subsurface soil—which has been previously demonstrated in other systems (e.g., Frey et al., 2003; Witzgall et al., 2021). Thus, our data expand the role of fungi beyond the spatial extension of the biocrust layer, emphasizing their importance as

biocrust components as well as their role in biogeochemical cycling in the subcrust soil (Abed et al., 2013).

Most strikingly, C and N accumulation in the 0–1 cm soil under ambient biocrusts was associated with an increase in mineral-associated OM (MAOM$_{<63\mu m}$; Figure 4). Similar to the linkage between fungal abundance and C and N accumulation in the biocrust layer, we found a strong correlation between C and N allocated in MAOM$_{<63\mu m}$ in the mineral soil and fungi:bacteria ratio. Thus, involvement of fungal networks not only drives the downward C translocation but also the formation of MAOM in the mineral soil, thereby marking an important contribution of biocrusts and the associated soil microbiome to the formation of organo-mineral assemblages in the mineral soil, which can potentially increase OM persistence (Lehmann et al., 2020). However, these processes are vulnerable to both drought and warming, even in the short term, emphasizing how changing climatic conditions may offset the contribution of biocrust-derived OM to the formation of more persistent soil C. To the best of our knowledge, this is the first time that the direct formation of MAOM has been demonstrated in soil separated from biocrusts (Figure 7).

5 | CONCLUSION

Biocrusts are widely recognized as key primary producers in drylands, affecting both C and N cycling at the ecosystem scale. With ongoing climate change and the associated expansion of arid lands, this increases the importance for a process-level understanding of the functionality of these systems, as a precondition to forecast ecological consequences on biocrust–soil interfaces under global change (Huang et al., 2016; Maestre et al., 2013; Rodríguez-Caballero et al., 2018).

We show how the impact of biocrusts can extend into the mineral soil, shaping a soil–microbial environment that facilitates downward C and N translocation and formation of MAOM in the subcrust soil, modulated mainly by the expansion of fungal hyphal networks. The high vulnerability of these systems to climate change was demonstrated by the impaired C and N accumulation and restricted MAOM formation. Under drought and warmer temperatures, C losses were intensified via accelerated C turnover and reduced efficiency of C uptake. Under drought specifically, this ultimately resulted in biocrusts no longer sustaining net C uptake as respiratory C losses increased while photosynthetic C uptake was constrained by the limited moisture. Overall, the induced climate change resulted in a reduced net biological N fixation by the biocrusts, which can have tremendous implications in otherwise N-limited dryland ecosystems. We further showed how biocrust–soil systems respond rapidly to changing environmental conditions, where some of the most fundamental biogeochemical processes—C and N pathways into more persistent SOM pools within the mineral soil—are diminished under short-term climate change (Figure 7).

Here, we provide a mechanistic framework for quantifying biogeochemical responses of soil–biocrust systems to changing climatic conditions, adding to the growing body of evidence that biocrusts may reach critical tipping points when exposed to climate change. This contributes to a deeper understanding of biocrust–soil dynamics under changing climatic conditions, which is fundamental for accurately predicting dynamics of dryland C cycling amidst ongoing global change.

AUTHOR CONTRIBUTIONS
K. Witzgall: Conceptualization; data curation; formal analysis; investigation; methodology; visualization; writing – original draft; writing – review and editing. **B. D. Hesse:** Conceptualization; data curation; formal analysis; investigation; methodology; writing – original draft; writing – review and editing. **N. L. Pacay-Barrientos:** Data curation; formal analysis; investigation; methodology; writing – review and editing. **J. Jansa:** Data curation; formal analysis; methodology; writing – review and editing. **O. Seguel:** Data curation; formal analysis; methodology; writing – review and editing. **R. Oses:** Data curation; investigation; writing – review and editing. **F. Buegger:** Data curation; methodology; writing – review and editing. **J. Guigue:** Data curation; methodology; writing – review and editing. **C. Rojas:** Conceptualization; data curation; writing – review and editing. **K. Rousk:** Conceptualization; supervision; writing – review and editing. **T. E. E. Grams:** Conceptualization; supervision; writing – review and editing. **N. Pietrasiak:** Conceptualization; supervision; writing – review and editing. **C. W. Mueller:** Conceptualization; funding acquisition; investigation; project administration; resources; supervision; writing – review and editing.

CONFLICT OF INTEREST STATEMENT
The authors declare no conflict of interest.

DATA AVAILABILITY STATEMENT

ORCID

K. Witzgall https://orcid.org/0000-0003-1366-9056
B. D. Hesse https://orcid.org/0000-0003-1113-9801
N. L. Pacay-Barrientos https://orcid.org/0009-0004-5464-9937
J. Jansa https://orcid.org/0000-0002-0331-1774
O. Seguel https://orcid.org/0000-0001-7040-3604
R. Oses https://orcid.org/0000-0003-2310-3339
F. Buegger https://orcid.org/0000-0003-3526-4711
J. Guigue https://orcid.org/0000-0001-8140-4450
C. Rojas https://orcid.org/0000-0001-7727-2862
K. Rousk https://orcid.org/0000-0003-3140-9864
T. E. E. Grams https://orcid.org/0000-0002-4355-8827
N. Pietrasiak https://orcid.org/0000-0003-4636-8006
C. W. Mueller https://orcid.org/0000-0003-4119-0544

REFERENCES

Übernickel, K., Ehlers, T. A., Ershadi, M. R., Paulino, L., Beer, A. R., Fuentes Espoz, J., Maldonado, A., Oses-Pedraza, R., & von Blanckenburg, F. (2020). Time series of meteorological station data in the EarthShape study areas in the coastal cordillera, Chile. V. 1.2. GFZ Data Services. https://doi.org/10.5880/fidgeo.2020.043

Abed, R. M., Al-Sadi, A. M., Al-Shehi, M., Al-Hinai, S., & Robinson, M. D. (2013). Diversity of free-living and lichenized fungal communities in biological soil crusts of the Sultanate of Oman and their role in improving soil properties. Soil Biology and Biochemistry, 57, 695–705. https://doi.org/10.1016/j.soilbio.2012.07.023

Amelung, W., & Zech, W. (1999). Minimisation of organic matter disruption during particle-size fractionation of grassland epipedons. Geoderma, 92(1–2), 73–85. https://doi.org/10.1016/S0016-7061(99)00023-3

Angst, G., Mueller, K. E., Nierop, K. G., & Simpson, M. J. (2021). Plant-or microbial-derived? A review on the molecular composition of stabilized soil organic matter. Soil Biology and Biochemistry, 156, 108189. https://doi.org/10.1016/j.soilbio.2021.108189

Barger, N. N., Herrick, J. E., Van Zee, J., & Belnap, J. (2006). Impacts of biological soil crust disturbance and composition on C and N loss from water erosion. Biogeochemistry, 77, 247–263. https://doi.org/10.1007/s10533-005-1424-7

Barger, N. N., Weber, B., Garcia-Pichel, F., Zaady, E., & Belnap, J. (2016). Patterns and controls on nitrogen cycling of biological soil crusts. In B. Weber, B. Büdel, & J. Belnap (Eds.), Biological soil crusts: An organizing principle in drylands. Ecological studies (Vol. 226). Springer. https://doi.org/10.1007/978-3-319-30214-0_14

Bates, S. T., Nash, T. H., III, Sweat, K. G., & Garcia-Pichel, F. (2010). Fungal Communities of Lichen-Dominated Biological Soil Crusts: Diversity, Relative Microbial Biomass, and Their Relationship to Disturbance and Crust Cover. Journal of Arid Environments, 74(10), 1192–1199. https://doi.org/10.1016/j.jaridenv.2010.05.033

Belnap, J. (2001). Factors influencing nitrogen fixation and nitrogen release in biological soil crusts. In J. Belnap & O. L. Lange (Eds.), Biological soil crusts: Structure, function, and management. Ecological studies (Vol. 150, pp. 241–261). Springer. https://doi.org/10.1007/978-3-642-56475-8_19

Belnap, J., & Lange, O. (2001). Biological soil crusts: Structure, function, and management. In O. L. Lange (Ed.), Ecological studies series (Vol. 150, pp. 241–261). Springer. https://doi.org/10.1007/978-3-642-56475-8

Belnap, J., Weber, B., & Büdel, B. (2016). Biological soil crusts as an organizing principle in drylands. Springer International Publishing.

Beraldi-Campesi, H., Hartnett, H. E., Anbar, A., Gordon, G. W., & Garcia-Pichel, F. (2009). Effect of biological soil crusts on soil elemental concentrations: Implications for biogeochemistry and as traceable biosignatures of ancient life on land. Geobiology, 7(3), 348–359. https://doi.org/10.1111/j.1472-4669.2009.00204.x

Bernhard, N., Moskwa, L. M., Schmidt, K., Oeser, R. A., Aburto, F., Bader, M. Y., Baumann, K., von Blanckenburg, F., Boy, J., van den Brink, L., Brucker, E., Büdel, B., Canessa, R., Dippold, M. A., Ehlers, T. A., Fuentes, J. P., Godoy, R., Jung, P., Karsten, U., & Kühn, P. (2018). Pedogenic and Microbial Interrelations to Regional Climate and Local Topography: New Insights from a Climate Gradient (Arid to Humid) Along the Coastal Cordillera of Chile. Catena, 170, 335–355. https://doi.org/10.1016/j.catena.2018.06.018

Bowling, D. R., Grote, E. E., & Belnap, J. (2011). Rain Pulse Response of Soil CO2 Exchange by Biological Soil Crusts and Grasslands of the Semiarid Colorado Plateau, United States. Journal of Geophysical Research: Biogeosciences, 116, G03028.

Bradford, M. A., Davies, C. A., Frey, S. D., Maddox, T. R., Melillo, J. M., Mohan, J. E., Reynolds, J. F., Treseder, K. K., & Wallenstein, M. D. (2008). Thermal Adaptation of Soil Microbial Respiration to Elevated Temperature. Ecology Letters, 11(12), 1316–1327. https://doi.org/10.1111/j.1461-0248.2008.01251.x

Castillo-Monroy, A. P., Maestre, F. T., Rey, A., Soliveres, S., & García-Palacios, P. (2011). Biological soil crust microsites are the main contributor to soil respiration in a semiarid ecosystem. Ecosystems, 14, 835–847. https://doi.org/10.1007/s10021-011-9449-3

Chamizo, S., Cantón, Y., Lázaro, R., Solé-Benet, A., & Domingo, F. (2012). Crust composition and disturbance drive infiltration through biological soil crusts in semiarid ecosystems. Ecosystems, 15, 148–161. https://doi.org/10.1007/s10021-011-9499-6

Chenu, C., & Cosentino, D. (2011). Microbial Regulation of Soil Structural Dynamics. In The Architecture and Biology of Soils: Life in Inner Space (pp. 37–70). CABI.

Coe, K. K., Belnap, J., & Sparks, J. P. (2012). Precipitation-driven carbon balance controls survivorship of desert biocrust mosses. Ecology, 93(7), 1626–1636. https://doi.org/10.1890/11-2247.1

Conant, R. T., Dalla-Betta, P., Klopatek, C. C., & Klopatek, J. M. (2004). Controls on Soil Respiration in Semiarid Soils. Soil Biology and Biochemistry, 36(6), 945–951. https://doi.org/10.1016/j.soilbio.2004.02.013

Costa, O. Y. A., Raaijmakers, J. M., & Kuramae, E. E. (2018). Microbial extracellular polymeric substances: Ecological function and impact on soil aggregation. Frontiers in Microbiology, 9, 1636. https://doi.org/10.3389/fmicb.2018.01636

Díaz-Martínez, P., Panettieri, M., García-Palacios, P., Moreno, E., Plaza, C., & Maestre, F. T. (2023). Biocrusts modulate climate change effects on soil organic carbon pools: Insights from a 9-year experiment. Ecosystems, 26(3), 585–596. https://doi.org/10.1007/s10021-022-00779-0

Dacal, M., Bradford, M. A., Plaza, C., Maestre, F. T., & García-Palacios, P. (2019). Soil microbial respiration adapts to ambient temperature in global drylands. Nature Ecology & Evolution, 3(2), 232–238. https://doi.org/10.1038/s41559-018-0770-5

Dacal, M., García-Palacios, P., Asensio, S., Cano-Díaz, C., Gozalo, B., Ochoa, V., & Maestre, F. T. (2020). Contrasting mechanisms underlie short-and longer-term soil respiration responses to experimental warming in a dryland ecosystem. Global Change Biology, 26(9), 5254–5266. https://doi.org/10.1111/gcb.15209

Darrouzet-Nardi, A., Reed, S. C., Grote, E. E., & Belnap, J. (2015). Observations of net soil exchange of CO_2 in a dryland show experimental warming increases carbon losses in biocrust soils. Biogeochemistry, 126, 363–378. https://doi.org/10.1007/s10533-015-0163-7

Davidson, E. A., Janssens, I. A., & Luo, Y. (2006). On the variability of respiration in terrestrial ecosystems: Moving beyond Q10. Global

Change Biology, *12*(2), 154–164. https://doi.org/10.1111/j.1365-2486.2005.01065.x

Elbert, W., Weber, B., Burrows, S., Steinkamp, J., Büdel, B., Andreae, M. O., & Pöschl, U. (2012). Contribution of cryptogamic covers to the global cycles of carbon and nitrogen. *Nature Geoscience*, *5*(7), 459–462. https://doi.org/10.1038/ngeo1486

Eliasson, P. E., McMurtrie, R. E., Pepper, D. A., Strömgren, M., Linder, S., & Ågren, G. I. (2005). The response of heterotrophic CO_2 flux to soil warming. *Global Change Biology*, *11*(1), 167–181. https://doi.org/10.1111/j.1365-2486.2004.00878.x

Fanin, N., Hättenschwiler, S., & Fromin, N. (2014). Litter fingerprint on microbial biomass, activity, and community structure in the underlying soil. *Plant and Soil*, *379*, 79–91. https://doi.org/10.1007/s11104-014-2051-7

Felde, V. J. M. N. L., Chamizo, S., Felix-Henningsen, P., & Drahorad, S. L. (2018). What stabilizes biological soil crusts in the Negev Desert? *Plant and Soil*, *429*, 9–18. https://doi.org/10.1007/s11104-017-3459-7

Ferrenberg, S., Faist, A. M., Howell, A., & Reed, S. C. (2018). Biocrusts enhance soil fertility and Bromus tectorum growth, and interact with warming to influence germination. *Plant and Soil, 429*, 77–90. https://doi.org/10.1007/s11104-017-3525-1

Ferrenberg, S., Reed, S. C., & Belnap, J. (2015). Climate change and physical disturbance cause similar community shifts in biological soil crusts. *Proceedings of the National Academy of Sciences of the United States of America*, *112*(39), 12116–12121. https://doi.org/10.1073/pnas.1509150112

Finger-Higgens, R., Duniway, M. C., Fick, S., Geiger, E. L., Hoover, D. L., Pfennigwerth, A. A., Scoyoc, M. W., & Belnap, J. (2022). Decline in biological soil crust N-fixing lichens linked to increasing summertime temperatures. *Proceedings of the National Academy of Sciences of the United States of America*, *119*(16), e2120975119. https://doi.org/10.1073/pnas.2120975119

Frey, S. D., Six, J., & Elliott, E. T. (2003). Reciprocal Transfer of Carbon and Nitrogen by Decomposer Fungi at the Soil–Litter Interface. *Soil Biology and Biochemistry*, *35*(7), 1001–1004. https://doi.org/10.1016/S0038-0717(03)00155-X

Garcia-Pichel, F., Loza, V., Marusenko, Y., Mateo, P., & Potrafka, R. M. (2013). Temperature drives the continental-scale distribution of key microbes in topsoil communities. *Science*, *340*(6140), 1574–1577. https://doi.org/10.1126/science.1236404

Hagemann, U., & Moroni, M. T. (2015). Moss and lichen decomposition in old-growth and harvested high-boreal forests estimated using the litterbag and minicontainer methods. *Soil Biology and Biochemistry*, *87*, 10–24. https://doi.org/10.1016/j.soilbio.2015.04.002

Hooper, D. U., & Johnson, L. (1999). Nitrogen limitation in dryland ecosystems: Responses to geographical and temporal variation in precipitation. *Biogeochemistry*, *46*, 247–293. https://doi.org/10.1007/BF01007582

Housman, D. C., Powers, H. H., Collins, A. D., & Belnap, J. (2006). Carbon and nitrogen fixation differ between successional stages of biological soil crusts in the Colorado plateau and Chihuahuan Desert. *Journal of Arid Environments*, *66*(4), 620–634. https://doi.org/10.1016/j.jaridenv.2005.11.014

Huang, J., Yu, H., Guan, X., Wang, G., & Guo, R. (2016). Accelerated dryland expansion under climate change. *Nature Climate Change*, *6*(2), 166–171. https://doi.org/10.1038/nclimate2837

Johnson, S. L., Budinoff, C. R., Belnap, J., & Garcia-Pichel, F. (2005). Relevance of ammonium oxidation within biological soil crust communities. *Environmental Microbiology*, *7*(1), 1–12. https://doi.org/10.1111/j.1462-2920.2004.00649.x

Kidron, G. J., Lichner, L., Fischer, T., Starinsky, A., & Or, D. (2022). Mechanisms for biocrust-modulated runoff generation—A review. *Earth-Science Reviews*, *231*, 104100. https://doi.org/10.1016/j.earscirev.2022.104100

Kidron, G. J., Vonshak, A., Dor, I., Barinova, S., & Abeliovich, A. (2010). Properties and spatial distribution of microbiotic crusts in the Negev Desert, Israel. *Catena*, *82*(2), 92–101. https://doi.org/10.1016/j.catena.2010.05.006

Kramer, C., & Gleixner, G. (2008). Soil organic matter in soil depth profiles: Distinct carbon preferences of microbial groups during carbon transformation. *Soil Biology and Biogeochemistry*, *40*, 425–433. https://doi.org/10.1016/j.soilbio.2007.09.016

Kriegler, F. J., Malila, W. A., Nalepka, R. F., & Richardson, W. (1969). Preprocessing transformations and their effect on multispectral recognition. *Remote Sensing of Environment*, *VI*, 97–132.

López-Mondéjar, R., Brabcová, V., Štursová, M., Davidová, A., Jansa, J., Cajthaml, T., & Baldrian, P. (2018). Decomposer food web in a deciduous forest shows high share of generalist microorganisms and importance of microbial biomass recycling. *The ISME Journal*, *12*(7), 1768–1778. https://doi.org/10.1038/s41396-018-0084-2

Ladrón de Guevara, M., Gozalo, B., Raggio, J., Lafuente, A., Prieto, M., & Maestre, F. T. (2018). Warming reduces the cover, richness and evenness of lichen-dominated biocrusts but promotes moss growth: Insights from an 8 yr experiment. *New Phytologist*, *220*(3), 811–823. https://doi.org/10.1111/nph.15000

Lange, O. L. (2001). Photosynthesis of soil-crust biota as dependent on environmental factors. In J. Belnap & O. L. Lange (Eds.), *Biological soil crusts: Structure, function, and management* (Vol. *150*, pp. 217–240). Springer. https://doi.org/10.1007/978-3-642-56475-8_18

Lehmann, J., Hansel, C. M., Kaiser, C., Kleber, M., Maher, K., Manzoni, S., Nunan, N., Reichstein, M., Schimel, J. P., Torn, M. S., Wieder, W. R., & Kögel-Knabner, I. (2020). Persistence of Soil Organic Carbon Caused by Functional Complexity. *Nature Geoscience*, *13*(8), 529–534. https://doi.org/10.1038/s41561-020-0612-3

Lenth, R. (2023). *emmeans: Estimated marginal means, aka least-squares means_*. R package version 1.8.8. https://CRAN.R-project.org/package=emmeans

Link, S. O., Smith, J. L., Halvorson, J. J., & Bolton, H., Jr. (2003). A reciprocal transplant experiment within a climatic gradient in a semiarid shrub-steppe ecosystem: Effects on bunchgrass growth and reproduction, soil carbon, and soil nitrogen. *Global Change Biology*, *9*(7), 1097–1105. https://doi.org/10.1046/j.1365-2486.2003.00647.x

Luebert, F., & Pliscoff, P. (2006). *Sinopsis bioclimática y vegetacional de Chile*. Editorial Universitaria.

Maestre, F. T., Cristina, E., Bardgett Richard, D., Dungait Jennifer, A. J., Beatriz, G., & Victoria, O. (2015). Warming reduces the cover and diversity of biocrust-forming mosses and lichens, and increases the physiological stress of soil microbial communities in a semi-arid *Pinus halepensis* plantation. *Frontiers in Microbiology*, *6*, 865. https://doi.org/10.3389/fmicb.2015.00865

Maestre, F. T., Delgado-Baquerizo, M., Jeffries, T. C., Eldridge, D. J., Ochoa, V., Gozalo, B., Quero, J. L., García-Gómez, M., Gallardo, A., Ulrich, W., Bowker, M. A., Arredondo, T., Barraza-Zepeda, C., Bran, D., Florentino, A., Gaitán, J., Gutiérrez, J. R., Huber-Sannwald, E., Jankju, M., & Singh, B. K. (2015). Increasing Aridity Reduces Soil Microbial Diversity and Abundance in Global Drylands. *Proceedings of the National Academy of Sciences of the United States of America*, *112*(5adap1), 15684–15689. https://doi.org/10.1073/pnas.1516684112

Maestre, F. T., Escolar, C., Ladrón de Guevara, M., Quero, J. L., Lázaro, R., Delgado-Baquerizo, M., Ochoa, V., Berdugo, M., Gozalo, B., & Gallardo, A. (2013). Changes in Biocrust Cover Drive Carbon Cycle Responses to Climate Change in Drylands. *Global Change Biology*, *19*(12), 3835–3847. https://doi.org/10.1111/gcb.12306

Mager, D. M. (2010). Carbohydrates in cyanobacterial soil crusts as a source of carbon in the southwest Kalahari, Botswana. *Soil Biology and Biochemistry*, *42*(2), 313–318. https://doi.org/10.1016/j.soilbio.2009.11.009

Mager, D. M., & Thomas, A. D. (2011). Extracellular polysaccharides from cyanobacterial soil crusts: A review of their role in dryland soil

processes. *Journal of Arid Environments*, 75(2), 91–97. https://doi.org/10.1016/j.jaridenv.2010.10.001

Maphangwa, K. W., Musil, C. F., Raitt, L., & Zedda, L. (2012). Experimental climate warming decreases photosynthetic efficiency of lichens in an arid South African ecosystem. *Oecologia*, 169(1), 257–268. https://doi.org/10.1007/s00442-011-2184-9

Mueller, C. W., Gutsch, M., Kothieringer, K., Leifeld, J., Rethemeyer, J., Brueggemann, N., & Kögel-Knabner, I. (2014). Bioavailability and isotopic composition of CO_2 released from incubated soil organic matter fractions. *Soil Biology and Biochemistry*, 69, 168–178. https://doi.org/10.1016/j.soilbio.2013.11.006

Permin, A., Horwath, A. B., Metcalfe, D. B., Priemé, A., & Rousk, K. (2022). High nitrogen-fixing rates associated with ground-covering mosses in a tropical mountain cloud forest will decrease drastically in a future climate. *Functional Ecology*, 36(7), 1772–1781. https://doi.org/10.1111/1365-2435.14088

Peterson, B. G., & Carl, P. (2020). *PerformanceAnalytics: Econometric tools for performance and risk analysis*. R package version 2.0.4. https://CRAN.R-project.org/package=PerformanceAnalytics

Pietrasiak, N., Regus, J. U., Johansen, J. R., Lam, D., Sachs, J. L., & Santiago, L. S. (2013). Biological soil crust community types differ in key ecological functions. *Soil Biology and Biochemistry*, 65, 168–171. https://doi.org/10.1016/j.soilbio.2013.05.011

Pinheiro, J., Bates, D., DebRoy, S., Sarkar, D., & R Core Team. (2024). Nlme: Linear and Nonlinear Mixed Effects Models. R package version, 3, 103. https://CRAN.R-project.org/package=nlme

Pointing, S. B., & Belnap, J. (2014). Disturbance to desert soil ecosystems contributes to dust-mediated impacts at regional scales. *Biodiversity and Conservation*, 23, 1659–1667. https://doi.org/10.1007/s10531-014-0690-x

Quideau, S. A., McIntosh, A. C., Norris, C. E., Lloret, E., Swallow, M. J., & Hannam, K. (2016). Extraction and analysis of microbial phospholipid fatty acids in soils. *Journal of Visualized Experiments*, 114, e54360. https://doi.org/10.3791/54360

Reed, S. C., Coe, K. K., Sparks, J. P., Housman, D. C., Zelikova, T. J., & Belnap, J. (2012). Changes to dryland rainfall result in rapid moss mortality and altered soil fertility. *Nature Climate Change*, 2(10), 752–755. https://doi.org/10.1038/nclimate1596

Riveras-Muñoz, N., Seitz, S., Witzgall, K., Rodríguez, V., Kühn, P., Mueller, C. W., Oses, R., Seguel, O., Wagner, D., & Scholten, T. (2022). Biocrust-linked changes in soil aggregate stability along a climatic gradient in the Chilean Coastal Range. *Soil Discussions*, 8, 717–731. https://doi.org/10.5194/soil-8-717-2022

Rodríguez, V., Bartholomäus, A., Witzgall, K., Riveras-Muñoz, N., Oses, R., Liebner, S., Kallmeyer, J., Rach, O., Mueller, C. W., Seguel, O., Scholten, T., & Wagner, D. (2024). Microbial Impact on Initial Soil Formation in Arid and Semiarid Environments Under Simulated Climate Change. *Frontiers in Microbiology*, 15, 1319997. https://doi.org/10.3389/fmicb.2024.1319997

Rodríguez-Caballero, E., Belnap, J., Büdel, B., Crutzen, P. J., Andreae, M. O., Pöschl, U., & Weber, B. (2018). Dryland photoautotrophic soil surface communities endangered by global change. *Nature Geoscience*, 11(3), 185–189. https://doi.org/10.1038/s41561-018-0072-1

Rossi, F., & De Philippis, R. (2015). Role of cyanobacterial exopolysaccharides in phototrophic biofilms and in complex microbial mats. *Life*, 5(2), 1218–1238. https://doi.org/10.3390/life5021218

Rousk, K., Sorensen, P. L., & Michelsen, A. (2018). What drives biological nitrogen fixation in high arctic tundra: Moisture or temperature? *Ecosphere*, 9(2), e02117. https://doi.org/10.1002/ecs2.2117

RStudio Team. (2015). *RStudio: Integrated development for R*. http://www.rstudio.com/

Samolov, E., Baumann, K., Büdel, B., Jung, P., Leinweber, P., Mikhailyuk, T., Karsten, U., & Glaser, K. (2020). Biodiversity of Algae and Cyanobacteria in Biological Soil Crusts Collected Along a Climatic Gradient in Chile Using an Integrative Approach. *Microorganisms*, 8(7), 1047. https://doi.org/10.3390/microorganisms8071047

Schimel, J. P. (2018). Life in dry soils: Effects of drought on soil microbial communities and processes. *Annual Review of Ecology, Evolution, and Systematics*, 49, 409–432. https://doi.org/10.1146/annurev-ecolsys-110617-062614

Sinsabaugh, R. L., Manzoni, S., Moorhead, D. L., & Richter, A. (2013). Carbon use efficiency of microbial communities: Stoichiometry, methodology and modelling. *Ecology Letters*, 16(7), 930–939. https://doi.org/10.1111/ele.12113

Smith, A. P., Bond-Lamberty, B., Benscoter, B. W., Tfaily, M. M., Hinkle, C. R., Liu, C., & Bailey, V. L. (2017). Shifts in pore connectivity from precipitation versus groundwater rewetting increases soil carbon loss after drought. *Nature Communications*, 8(1), 1335. https://doi.org/10.1038/s41467-017-01320-x

Swenson, T. L., Karaoz, U., Swenson, J. M., Bowen, B. P., & Northen, T. R. (2018). Linking soil biology and chemistry in biological soil crust using isolate exometabolomics. *Nature Communications*, 9(1), 19. https://doi.org/10.1038/s41467-017-02356-9

Teixeira, P. P. C., Trautmann, S., Buegger, F., Felde, V. J. M. N. L., Pausch, J., Mueller, C. W., & Kögel-Knabner, I. (2023). Role of root hair elongation in rhizosheath aggregation and in the carbon flow into the soil. *Biology and Fertility of Soils*, 59(3), 351–361. https://doi.org/10.1007/s00374-023-01708-6

Tucker, C., Ferrenberg, S., & Reed, S. C. (2020). Modest residual effects of short-term warming, altered hydration, and biocrust successional state on dryland soil heterotrophic carbon and nitrogen cycling. *Frontiers in Ecology and Evolution*, 8, 467157. https://doi.org/10.3389/fevo.2020.467157

Tucker, C. L., Bell, J., Pendall, E., & Ogle, K. (2013). Does declining carbon-use efficiency explain thermal acclimation of soil respiration with warming? *Global Change Biology*, 19(1), 252–263. https://doi.org/10.1111/gcb.12036

Tucker, C. L., Ferrenberg, S., & Reed, S. C. (2019). Climatic sensitivity of dryland soil CO_2 fluxes differs dramatically with biological soil crust successional state. *Ecosystems*, 22, 15–32. https://doi.org/10.1007/s10021-018-0250-4

Tucker, C. L., & Reed, S. C. (2016). Low soil moisture during hot periods drives apparent negative temperature sensitivity of soil respiration in a dryland ecosystem: A multi-model comparison. *Biogeochemistry*, 128, 155–169. https://doi.org/10.1007/s10533-016-0200-1

Vidal, A., Klöffel, T., Guigue, J., Angst, G., Steffens, M., Hoeschen, C., & Mueller, C. W. (2021). Visualizing the transfer of organic matter from decaying plant residues to soil mineral surfaces controlled by microorganisms. *Soil Biology and Biochemistry*, 160, 108347. https://doi.org/10.1016/j.soilbio.2021.108347

Weber, B., Belnap, J., Büdel, B., Antoninka, A. J., Barger, N. N., Chaudhary, V. B., Darrouzet-Nardi, A., Eldridge, D. J., Faist, A. M., Ferrenberg, S., Havrilla, C. A., Huber-Sannwald, E., Issa, O. M., Maestre, F. T., Reed, S. C., Rodriguez-Caballero, E., Tucker, C., Young, K. E., Zhang, Y., & Bowker, M. A. (2022). What Is a Biocrust? A Refined, Contemporary Definition for a Broadening Research Community. *Biological Reviews*, 97(5), 1768–1785. https://doi.org/10.1111/brv.12862

Weber, B., Bowker, M. A., Zhang, Y. M., & Belnap, J. (2016). Natural recovery of biological soil crusts after disturbance. In B. Weber, B. Büdel, & J. Belnap (Eds.), *Biological soil crusts: An organizing principle in drylands*. Ecological studies series (pp. 479–498). Springer-Verlag. https://doi.org/10.1007/978-3-319-30214-0_1

Witzgall, K., Hesse, B. D., Pacay-Barrientos, N., Jansa, J., Seguel, O., Oses, R., Buegger, F., Guigue, J., Rojas, C., Rousk, K., Grams, T. E. E., Pietrasiak, N., & Mueller, C. W. (2024). Dataset: Soil carbon and nitrogen cycling at the atmosphere-soil interface: Quantifying the responses of biocrust-soil interactions to global change. *Dryad Digital Repository*, https://doi.org/10.5061/dryad.h9w0vt4rp

Witzgall, K., Hesse, B. D., Seguel, O., Oses, R., Grams, T. E. E., & Mueller, C. W. (2023). Tracing low-CO_2 fluxes in soil incubation and ^{13}C labeling experiments: A simplified gas sampling system for respiration

and photosynthesis measurements. *Journal of Geophysical Research: Biogeosciences*, *128*(9), e2023JG007410. https://doi.org/10.1029/2023JG007410

Witzgall, K., Vidal, A., Schubert, D. I., Höschen, C., Schweizer, S. A., Buegger, F., Pouteau, V., Chenu, C., & Mueller, C. W. (2021). Particulate Organic Matter as a Functional Soil Component for Persistent Soil Organic Carbon. *Nature Communications*, *12*(1), 1–10. https://doi.org/10.1038/s41467-021-24192-8

Xiao, B., & Veste, M. (2017). Moss-dominated biocrusts increase soil microbial abundance and community diversity and improve soil fertility in semi-arid climates on the loess plateau of China. *Applied Soil Ecology*, *117*, 165–177. https://doi.org/10.1016/j.apsoil.2017.05.005

Xu, H., Zhang, Y., Shao, X., & Liu, N. (2022). Soil Nitrogen and Climate Drive the Positive Effect of Biological Soil Crusts on Soil Organic Carbon Sequestration in Drylands: A Meta-Analysis. *Science of the Total Environment*, *803*, 150030. https://doi.org/10.1016/j.scitotenv.2021.150030

Young, K. E., Ferrenberg, S., Reibold, R., Reed, S. C., Swenson, T., Northen, T., & Darrouzet-Nardi, A. (2022). Vertical movement of soluble carbon and nutrients from biocrusts to subsurface mineral soils. *Geoderma*, *405*, 115495. https://doi.org/10.1016/j.geoderma.2021.115495

SUPPORTING INFORMATION

Additional supporting information can be found online in the Supporting Information section at the end of this article.

How to cite this article: Witzgall, K., Hesse, B. D., Pacay-Barrientos, N. L., Jansa, J., Seguel, O., Oses, R., Buegger, F., Guigue, J., Rojas, C., Rousk, K., Grams, T. E. E., Pietrasiak, N., & Mueller, C. W. (2024). Soil carbon and nitrogen cycling at the atmosphere–soil interface: Quantifying the responses of biocrust–soil interactions to global change. *Global Change Biology*, *30*, e17519. https://doi.org/10.1111/gcb.17519